

Fall 2021

Integration of Process Planning Into the Automated Fiber Placement Design for Manufacturing Cycle

Alex Brasington

Follow this and additional works at: <https://scholarcommons.sc.edu/etd>



Part of the [Aerospace Engineering Commons](#)

Recommended Citation

Brasington, A.(2021). *Integration of Process Planning Into the Automated Fiber Placement Design for Manufacturing Cycle*. (Master's thesis). Retrieved from <https://scholarcommons.sc.edu/etd/6639>

This Open Access Thesis is brought to you by Scholar Commons. It has been accepted for inclusion in Theses and Dissertations by an authorized administrator of Scholar Commons. For more information, please contact digres@mailbox.sc.edu.

INTEGRATION OF PROCESS PLANNING INTO THE AUTOMATED FIBER
PLACEMENT DESIGN FOR MANUFACTURING CYCLE

by

Alex Brasington

Bachelor of Science
University of South Carolina, 2019

Submitted in Partial Fulfillment of the Requirements

For the Degree of Master of Science in

Aerospace Engineering

College of Engineering and Computing

University of South Carolina

2021

Accepted by:

Ramy Harik, Director of Thesis

Paul Ziehl, Reader

Tracey L. Weldon, Interim Vice Provost and Dean of the Graduate School

© Copyright by Alex Brasington, 2021
All Rights Reserved.

ACKNOWLEDGEMENTS

I would like to begin by thanking my advisor Dr. Ramy Harik. He has provided me the opportunity to be a part of his research team at the McNair Center, guidance not only professionally but personally, and unconditional support throughout my master's studies. I would also like to thank my committee member Dr. Paul Ziehl who has provided me with knowledge and guidance since my undergraduate studies. Additionally, I would like to express my gratitude to my fellow researchers who have provided me with advice, assistance, and feedback. This work would not be possible without the great team that I have had the chance to be a part of and contribute to.

ABSTRACT

Automated Fiber Placement (AFP) is a composite manufacturing technique utilizing a robotic or gantry-based system and an attached fiber placement head to lay a prescribed number of strips of composite material, additively forming large composite structures. This technique has enabled increased throughput with increased accuracy and reliability when compared with prior composite manufacturing methods. However, even with the current state-of-the-art AFP process which employs advanced computer simulations and complex robotic operations, the data from various levels of the manufacturing lifecycle is isolated. This results in an incoherent system between the initial design phase and final part completion with limited ability to progressively enhance the design. This thesis aims to begin the integration of data across multiple product lifecycle levels with the creation of a tool to incorporate process planning into the design for manufacturing cycle while also establishing a connection between the simulation environment and reality with a digital twin (DT). These tools enable a manufacturing informed design by analyzing prior, expected, and actual manufacturing data. To demonstrate the benefits of such an integration, an in-depth parametric study of a strut and airfoil shape is used.

TABLE OF CONTENTS

Acknowledgements	iii
Abstract	iv
Table of Contents	v
List of Tables	vii
List of Figures	viii
List of Abbreviations	xi
Chapter 1 Introduction	1
1.1 Preamble	1
1.2 AFP Process Description	2
1.3 History of AFP Developments	3
1.4 AFP Lifecycle Connection	6
1.5 Thesis Outline	10
Chapter 2 Literature Review	11
2.1 Design of Composite Materials	11
2.2 Layup strategies	14
2.3 Process Parameters	16
2.4 AFP Defects	19
2.5 Design and Process Planning Data Connection	30
2.6 Digital Twins in the Composites Industry	31
Chapter 3 Development of Data Integration Tools	33

3.1 AFP Phase Integration Tool	33
3.2 Data Structure.....	34
3.3 Software Interface	36
3.4 Functionalities	42
3.5 Manufacturability Analysis	50
3.6 Digital Twin Creation.....	54
3.7 Summary	56
Chapter 4 Experimental Validation Plan	58
4.1 Test Matrices	58
4.2 Strut Experiments	58
4.3 Airfoil Experiments	60
4.4 Manufacturability Ranking Strategy	63
4.5 Digital Twin Implementation	65
4.6 Summary	65
Chapter 5 Experimentation Results	66
5.1 Strut Experiment Results.....	66
5.2 Airfoil Experiment Results.....	72
5.3 Summary	80
Chapter 6 Conclusions and Future Work.....	82
6.1 Summary of Work	82
6.2 Future Work	83
6.3 Situation of Research	84
References.....	86

LIST OF TABLES

Table 2.1: Typical design practices for design of composite structures [21], [25].....	13
Table 2.2: List of defect types and their associated category [91].....	20
Table 4.1: Description of each variable for the strut trials	59
Table 4.2: Test matrix for examining chord length and thickness of the airfoil.....	61
Table 4.3: Test matrix for examining twist and taper of the airfoil	62
Table 4.4: Test matrix for examining airfoil thickness and twist angle.....	63
Table 4.5: Defect threshold values used for experiments	64
Table 4.6: AHP rankings for each defect category used for experiments	64
Table 5.1: Average ply scores for the 4 tow strut trials	67
Table 5.2: Average laminate scores for the 4 tow strut trials	67
Table 5.3: Average ply scores the 2 tow strut trials.....	69
Table 5.4: Average laminate scores for the 2 tow strut trials	69
Table 5.5: Combined results for strut trials with 2 and 4 tows	70
Table 5.6: Average ply scores for airfoil twist-taper study	74
Table 5.7: Average laminate scores for airfoil twist-taper study	74
Table 5.8: Average ply scores for airfoil thickness-twist study.....	76
Table 5.9: Average laminate scores for airfoil thickness-twist study	77

LIST OF FIGURES

Figure 1.1: Examples of a (a) robotic and (b) gantry style AFP machine	3
Figure 1.2: Timeline of AFP developments [19]	5
Figure 1.3: Anticipated workflow for industry 4.0 AFP [20]	6
Figure 1.4: Data connection of design and process planning	7
Figure 1.5: Data connection of process planning and manufacturing	8
Figure 1.6: Data connection of manufacturing and inspection	9
Figure 1.7: Data connection of inspection and design	9
Figure 2.1: CAD representation of a gap and overlap defect	22
Figure 2.2: CAD representation of a twist defect	23
Figure 2.3: CAD representation of a missing tow	23
Figure 2.4: CAD representation of a boundary coverage defect	24
Figure 2.5: CAD representation of an angle deviation defect	24
Figure 2.6: CAD representation of a wandering tow	25
Figure 2.7: CAD representation of a position error defect	26
Figure 2.8: CAD representation of a fold	26
Figure 2.9: CAD representation of a pucker defect	27
Figure 2.10: CAD representation of a wrinkle.....	27
Figure 2.11: CAD representation of bridging	28
Figure 2.12: CAD representation of a loose tow defect.....	29
Figure 2.13: CAD representation of a splice	29

Figure 2.14: CAD representation of FOD.....	30
Figure 3.1: Breakdown of the data structure within neXtC	35
Figure 3.2: neXtC software layout.....	37
Figure 3.3: Description of the laminate tree	38
Figure 3.4: Buttons with the (a) design, (b) process planning, and (c) manufacturing tabs.....	40
Figure 3.5: Data analysis viewers for (a) design and (b) process planning data	41
Figure 3.6: Interface viewing related buttons	41
Figure 3.7: Buttons to control project data	41
Figure 3.8: Surface import dialog box	42
Figure 3.9: User input boxes for creating (a) strut geometry and (b) plies.....	43
Figure 3.10: Example of tool surface curvature analysis.....	44
Figure 3.11: Example of (a) surface splitting, (b) meshing and HKS, and (c) scenario creation in the CAPP process	45
Figure 3.12: User selection of layup strategies	45
Figure 3.13: Histogram representation of defect data.....	46
Figure 3.14: Feature threshold value chart	47
Figure 3.15: AHP matrix and rankings	47
Figure 3.16: User interface to select scenarios to export	49
Figure 3.17: Description of courses for PS	49
Figure 3.18: Graphical comparison of manufacturability of (a) laminates and (b) plies.....	50
Figure 3.19: Numerical comparison of manufacturing of (a) laminates and (b) plies.....	50
Figure 3.20: Splitting of the surface and defects	51
Figure 3.21: Example of the manufacturability section analysis of the tool surface	53

Figure 3.22: Manufacturability correlation matrix	54
Figure 3.23: Comparison of the (a) physical and (b) digital ISAAC AFP machine	55
Figure 3.24: Kinematic setup of the AFP machine.....	55
Figure 3.25: TCP location on the AFP head	56
Figure 4.1: Graphical representation of the strut trials matrix.....	59
Figure 4.2: Airfoil shape for examining thickness vs. chord length.....	60
Figure 4.3: Airfoil shape with variations in twist and taper	61
Figure 4.4: Airfoil shape with variation in thickness and twist	63
Figure 5.1: Ply and laminate scores for the 4 tow strut trials	66
Figure 5.2: Trends in the laminate scores for the 4 tow strut trials	68
Figure 5.3: Ply and laminate score for the 2 tow strut trials	68
Figure 5.4: Trends in laminate scores for the 2 tow strut trials	70
Figure 5.5: Defect analysis from VCP for 45-degree plies of (a) 4 tow and (b) 2 tow strut trials.....	71
Figure 5.6: Selected strut geometry with the overall best results	72
Figure 5.7: Ranking of each ply angle for the twist-taper airfoil study	73
Figure 5.8: Manufacturability correlation graph for airfoil twist-taper study	75
Figure 5.9: Ranking of each ply angle for the thickness-twist airfoil study	76
Figure 5.10: Manufacturability correlation graph for airfoil thickness-twist study.....	77
Figure 5.11: Local analysis of (a) overlaps, (b) gaps, (c) angle deviations, and (d) steering.....	79
Figure 5.12: Airfoil parametric study correlation matrix.....	80
Figure 5.13: Depiction of the data connection between design and process planning.....	81
Figure 6.1: neXtC software interface.....	83

LIST OF ABBREVIATIONS

AFP	Automated Fiber Placement
AHP.....	Analytic Hierarchy Process
ATL.....	Automated Tape Laying
CAD	Computer Aided Design
CAPP.....	Computer Aided Process Planning
CFRP.....	Carbon Fiber Reinforced Plastic
EI.....	Electroimpact
FOD.....	Foreign Object Debris
FW.....	Filament Winding
GFRP.....	Glass Fiber Reinforced Plastic
HKS.....	Heat Kernel Signature
ISAAC.....	Integrated Structural Assembly of Advanced Composites
LaRC	Langley Research Center
ML.....	Machine Learning
neXtC	neXt Composites
PLM	Product Lifecycle Management
PS	Process Simulate
UofSC	University of South Carolina
UI	User Interface
VCP.....	VERICUT Composites Programming

CHAPTER 1

INTRODUCTION

1.1 PREAMBLE

Carbon fiber materials became available for commercial use in 1966 stemming from research done by Watt et al. at the Royal Aircraft Establishment [1], [2]. These materials became largely prevalent in the aerospace industry due to their ability to create lightweight structures with superior qualities when compared to those made of traditional materials such as metal or wood. Recent developments in the constituent materials have expanded the use cases of composite materials to several other industries such as automotive, renewable energy, and civil engineering applications. This has led to the need for innovative manufacturing techniques to withstand the ever-increasing throughput requirement.

Initial manufacturing techniques consisted mostly of hand layup with glass-fiber reinforced plastics (GFRP) and carbon fiber reinforced plastics (CFRP). This method requires manual cutting and placing of composite materials onto an open mold. Personnel must closely follow manufacturing guidelines along with utilizing an appropriate stacking sequence to achieve the desired quality and mechanical properties. Obviously, this process can lead to defects due to a multitude of factors such as human error or complexity of the layup surface. Further, the throughput of this technique is not near what is required for current and future manufacturing.

Due to the increased reliability and throughput required by composite manufacturing techniques, automation was incorporated. Before AFP technologies were created, composite production of large structures was largely accomplished with automated tape laying (ATL) and filament winding (FW). The earliest documented account of the concept of using tows instead of tapes was a patent by Goldsworth et al. in 1974 [3]. This invention utilized a splitting mechanism on an ATL head that slit 3-inch-wide tapes into 24 individual strands, now referred to as tows. The use of tows allowed for layup on increasingly complex parts that were not previously possible with wider tapes. The use of such a slitting mechanism led the way for future developments leading up to the AFP machine.

1.2 AFP PROCESS DESCRIPTION

AFP is a recently established manufacturing technique that was developed less than 30 years ago. The AFP process consists of a gantry/robotic system with an attached fiber placement head. This head enables multiple strips of composite material, or tows, to be laid onto a tool surface. Adhesion between the incoming tows and substrate is ensured by using appropriate process conditions such as heating, compaction, and tow tension. A series of tows forms a course, courses are then combined to create a ply, and multiple plies create a laminate. An example of a robotic style Integrated Structural Assembly of Advanced Composites (ISAAC) AFP machine developed by EI located at NASA Langley Research Center (LaRC) and an Ingersoll Machine Tools (IMT) Lynx gantry style machine at the University of South Carolina's (UofSC) McNAIR Center are present in Figure 1.1 below. The following will provide a brief history of AFP and its major advancements.

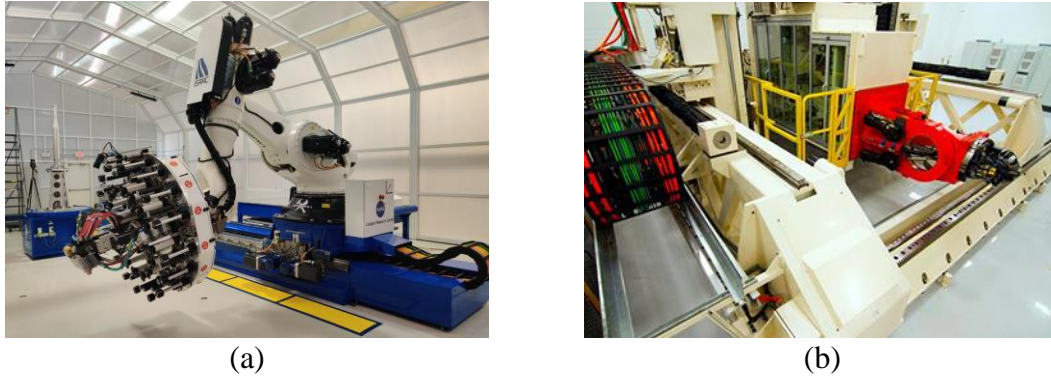


Figure 1.1: Examples of a (a) robotic and (b) gantry style AFP machine

1.3 HISTORY OF AFP DEVELOPMENTS

Hercules began development of AFP machines in 1980, and they became commercially available later that decade, being implemented by aerospace companies such as Boeing, Lockheed, and Northrop [4]. The machines were a combination of the differential payout capability of filament winding and the compaction and cut-restart capabilities of ATL. The AFP system had the capability to vary layup speed, pressure, temperature, and tow tension. Bullock added to this capability by demonstrating an offline programming system that would benefit the production time of the machine [5]. The offline system allowed the programming to be done independently and then uploaded to the machine for execution.

A report by Grant and Benson in 1993 presented the implementation of a refrigerated creel system to minimize issues within the creel, prolong material life, and allow for clean unspooling [6]. Research in the 1990's was also focused on improving productivity of the AFP process. This began with a system that could deliver up to 24 tows at once [7]. With this system a layup rate of up to 30 m/min was reported, corresponding to a productivity of 1.9 kg/hr, more than doubling the productivity associated with manual

layup. Productivity continued to enhance through improved process reliability [8]. Reliability over complex geometries was improved by delivering tows along a curvilinear path, otherwise known as steering. An application of this development showed a 450% improvement in productivity, a reduced material wastage from 62% to 6%, and a cost reduction of 43% when compared with using a combination of filament winding and hand layup [9, 10]. These improvements in AFP also coincided with the development of thermoplastic composites for aerospace structural applications. The use of these materials allowed for in-situ consolidation during layup, but higher placement temperatures and pressures are required [11]. Research on thermoplastic layups became a necessity due to the size of large aircraft and submarines exceeding the size of the autoclaves needed for curing [12].

Starting in the 2000's a significant portion of research was focused on continuing improvement of process reliability and productivity. Boeing [13] and Electroimpact (EI) [14] have performed studies on the amount of time delegated to inspection and rework of AFP layups. Boeing showed that layup inspection and rework comprised 63% of the total time, more than 2.5 times as long as the layup process. Electroimpact (EI) found that inspection and repair consumed 32% of the total time, while machine layup time was 27%. A 2006 patent produced by Engelbart et al. was the first to describe an automated detection system [15]. The system would electronically access positional data to define a defect location, and then the machine would automatically return to that location. EI also made a major contribution to the productivity of AFP machine with the development of a high-speed system capable of 2000 in/min (50.8 m/min) with interchangeable heads and reduced tow-path length [16].

Research by Flynn et al. published in the 2010 presented efficient simultaneous use of a multiple machine cell as well as modular AFP heads [17]. The modular head offered advantages of 360-degree positioning, multiplicity of tow widths, short tow path, and offline maintenance. This was further enhanced with a report in 2013 with highly accurate robots demonstrating a 3-sigma accuracy of ± 0.08 mm [18].

The most recent industry relevant AFP research topics consist of high throughput AFP, minimal defect layups, and in-situ thermoplastic layups. High throughput AFP and minimal defect layups are focused on improving the overall quality and efficiency of AFP manufactured structures. In-situ thermoplastic layups are focused on combining layup and curing, preventing the need to perform a costly and size limiting curing step. All the advancements presented in this section are summarized with a timeline below in Figure 1.2.

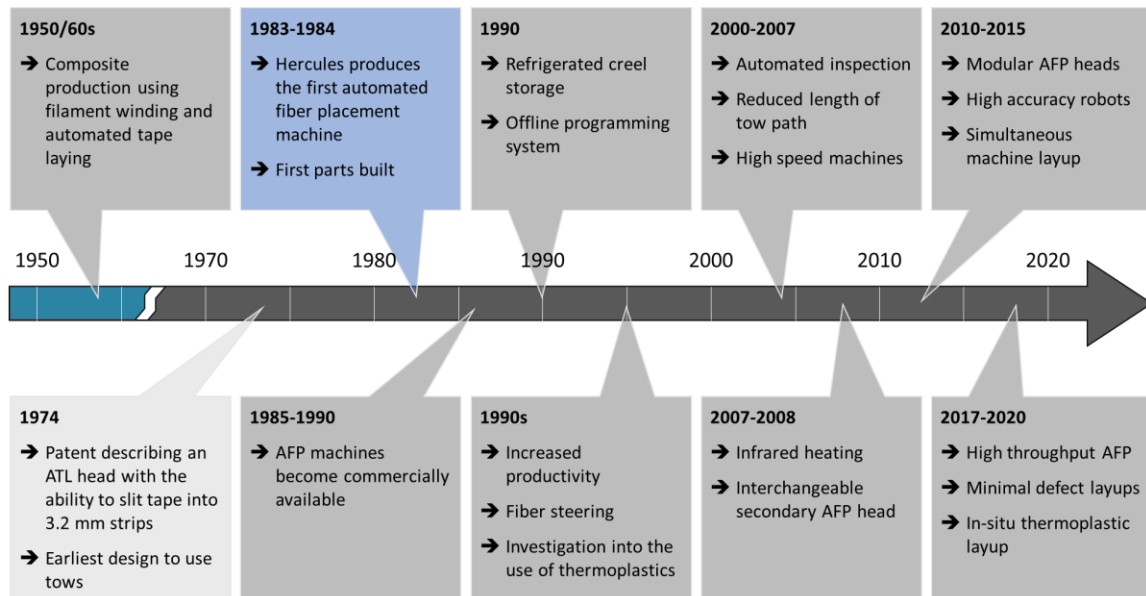


Figure 1.2: Timeline of AFP developments [19]

1.4 AFP LIFECYCLE CONNECTION

As technologies continually improve, composites manufacturing is in a race to integrate currently available digital technologies. For overall success, the integration must be intelligent, connected, and have the fundamental fabrication pillars communicate with each other. Those pillars being design, process planning, manufacturing, and inspection. Figure 1.3 below describes the complete vision of what an industry 4.0 AFP workflow would look like with seamless connections between all pillars [20]. This flow ensures that design is no longer a starting point, but rather a trade in a continuous improvement cycle that integrates process planning, manufacturing, and inspection. This thesis will not complete this entire cycle but serve as a starting point by initiating the connection of the design and process planning phase (Figure 1.4), along with beginning the connection between process planning and manufacturing (Figure 1.5).

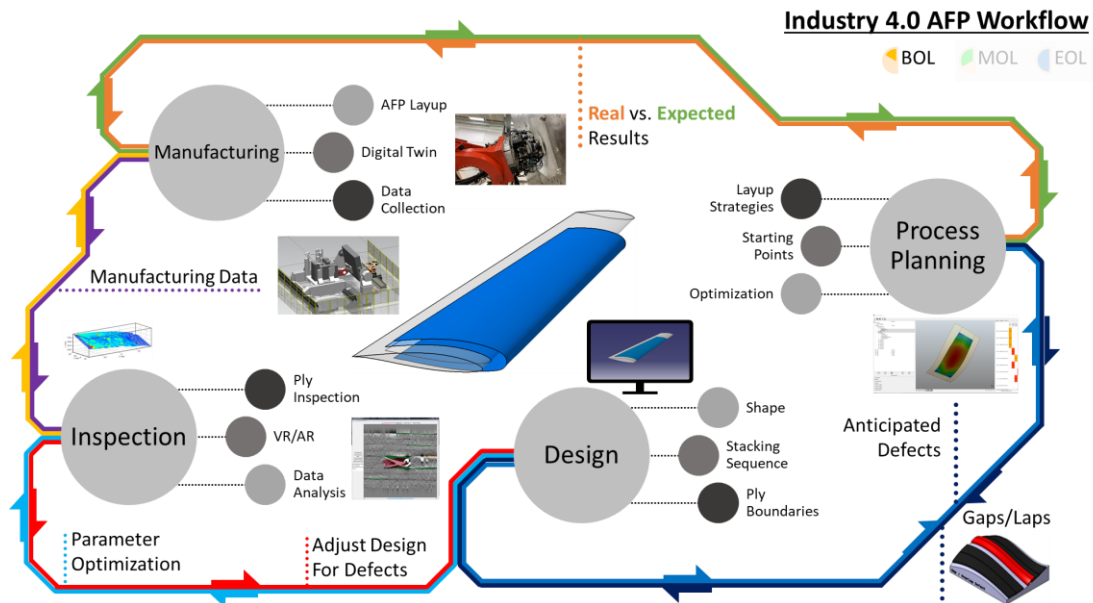


Figure 1.3: Anticipated workflow for industry 4.0 AFP [20]

At the stage of the workflow presented in Figure 1.4, design has communicated back and forth with process planning and a resultant toolpath with expected empirical results has been generated. The task of matchmaking the designed part with an acceptable manufacturing process is often left up to the process planner, leading to a back and forth to achieve an optimal part. Data sharing at this phase can eliminate the highly prevalent issue of designers failing to account for manufacturing limitations and streamline getting the part from the designer to the manufacturing floor.

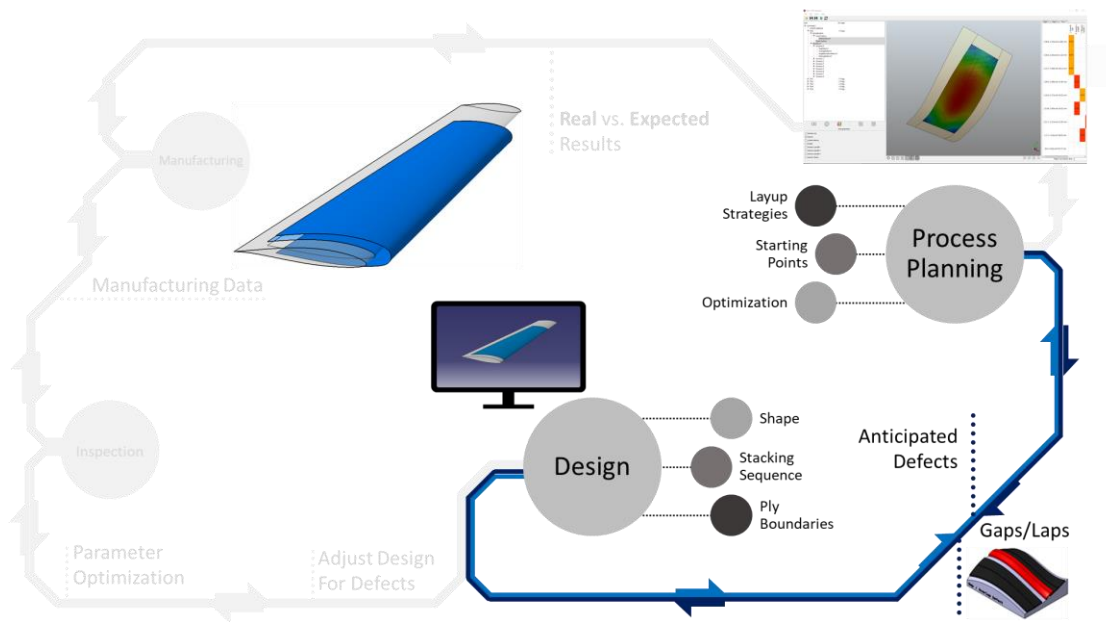


Figure 1.4: Data connection of design and process planning

The next stage of the workflow connects process planning and manufacturing. At this stage of the AFP process, design and process planning have had sufficient back and forth to generate an expected optimal manufacturing plan. Manufacturing is performed while collecting large amounts of data to be communicated to the machine's digital twin. The main concept of utilizing a digital twin is that the machine can draw the operation data and perform data analysis to propose changes in the manufacturing process. This will

require major integration of new automation hardware that can rapidly react to a complex domain with ever-changing material properties and requirements.

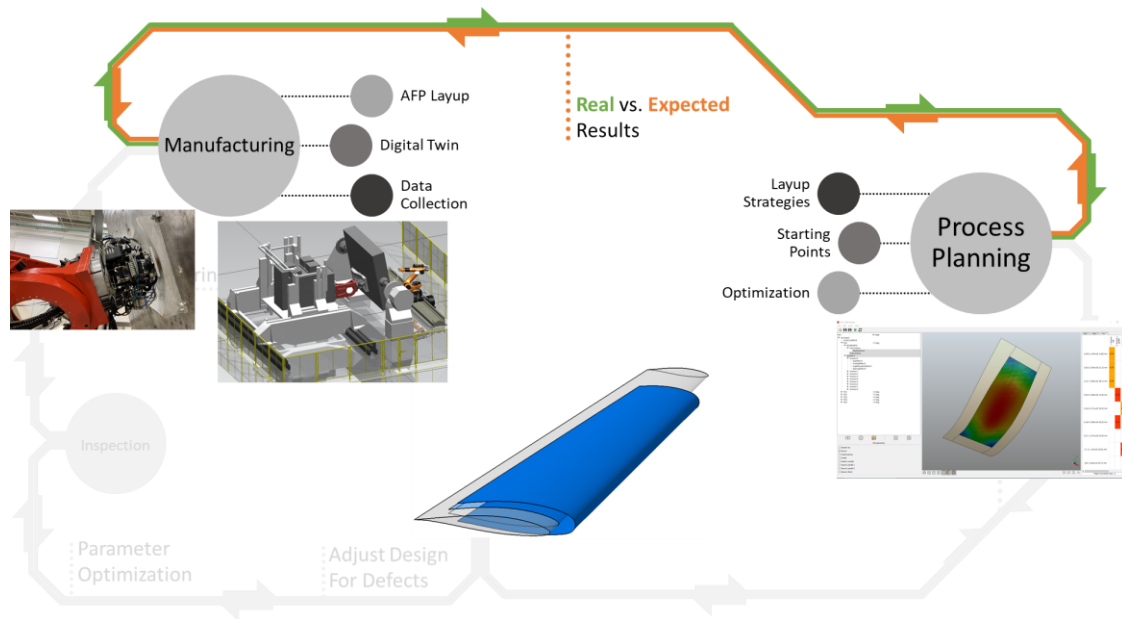


Figure 1.5: Data connection of process planning and manufacturing

The next stage of integration is connecting manufacturing with inspection. In this stage connections between layup data and the resulting defects are correlated. This builds on the continuous effort to create a data-driven composites manufacturing approach. The functionalities within this stage also include the representation of data into a virtual or augmented reality world that assists personnel with inspection tasks.

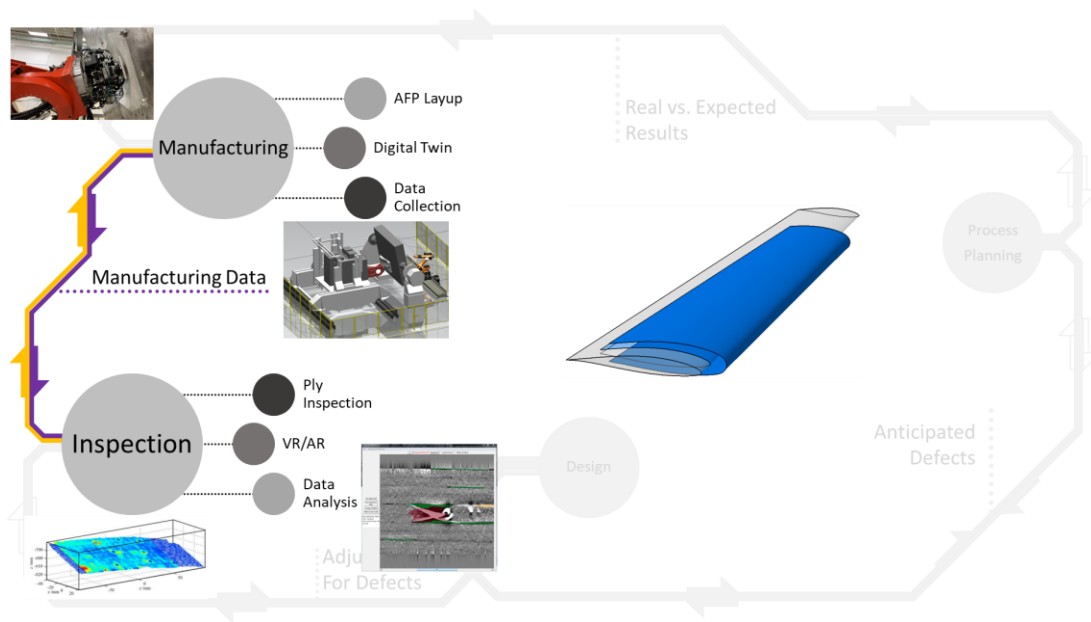


Figure 1.6: Data connection of manufacturing and inspection

Finally, the loop is closed with the connection of inspection and design. The data from the inspection is correlated to design resulting in optimization of the design parameters. With this connection, a closed loop AFP workflow is achieved.

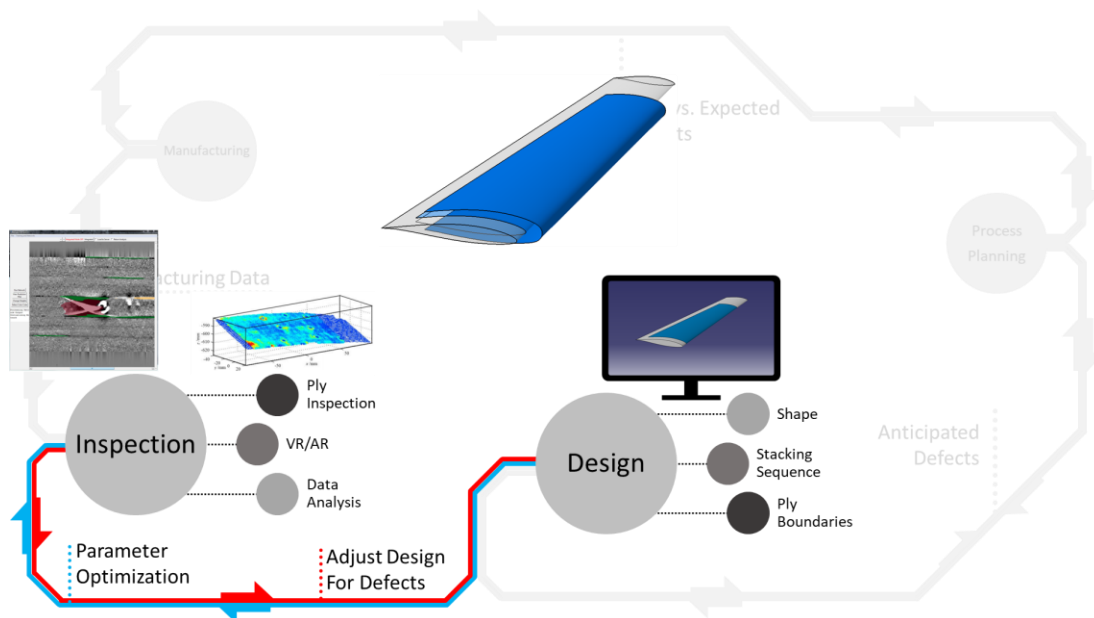


Figure 1.7: Data connection of inspection and design

1.5 THESIS OUTLINE

With the current state of AFP, the lifecycle continues to have an issue of data integration over the entire process. Even with the workflow presented above, the backbone for such a process is not present. This thesis aims to create such a process by initiating the creation of a product lifecycle management (PLM) software for AFP beginning with the data connection between design and process planning. The remainder of this thesis is organized as follows:

Chapter 2 presents a literature review of the aspects involved in the key AFP phases to be integrated (design and process planning). A review of digital twin applications in the composite industry is then presented.

Chapter 3 describes the development of the AFP software and the digital twin created at NASA LaRC. Each of the functions associated with these is detailed.

Chapter 4 details the test matrices used to evaluate the developed tools.

Chapter 5 presents the results from the tests performed and proves the validation of the developed software.

Chapter 6 concludes the works and presents future paths forward.

CHAPTER 2

LITERATURE REVIEW

2.1 DESIGN OF COMPOSITE MATERIALS

Composite materials have the advantage of improved mechanical properties such as high specific stiffness and strength, corrosion resistance, enhanced fatigue life, and improved fracture toughness [21]. However, utilizing the benefits of composites requires careful design and optimization. Setoodeh et al. [22], provides two categories of design of a composite structure: (1) constant stiffness [23] and (2) variable stiffness [24], [25]. A constant stiffness design uses the same stacking sequence over an entire structure where the goal of the design process is to optimize this sequence. Contrarily, a variable stiffness design utilizes changes in fiber angle across a structure where the varying fiber angles are optimized for structural performance.

In industry, manufacturing of composites is still limited to conventional constant stiffness laminates with possible fiber angles restricted to 0, ± 45 , and 90 degrees [26]. These fiber angles are often used in a way that creates a quasi-isotropic laminate. In addition to ply angle restrictions, laminate design guidelines have also been developed over time to guarantee the robustness of the laminate. These guidelines consist of having mid-plane symmetric laminates, balanced laminates, maximum number of consecutive plies, maximum and minimum ply angle jump, and ± 45 -degree surface plies [25]. Utilizing

symmetric and balance laminates minimizes of [B] matrix of the ABD matrix, resulting in avoided bending, coupling, warping, and twisting effects. The maximum number of consecutive plies should be limited to 2-4 layers which decreases the chance of delamination. The maximum jump of ply angles between plies decreases the inter-laminar stresses. Minimum ply angle jumps are used to obtain dispersed laminates, helping to withstand impacts. Further, utilizing ± 45 -degree surface layers improve damage tolerance, buckling load of thin laminates, and protect primary load carrying plies. Utilizing fabric plies as inner and outer layers can absorb more impact damage and can minimize drilling “breakout”. Lastly, it is advisable to use a larger fraction of ± 45 plies in shear regions because they handle shear loads better.

Design flexibility of composite structures can be enlarged by properly utilizing the fiber steering capabilities of a fiber placement machine, creating more efficient composite structures [27]. The advantage of curvilinear fibers on structural performance has been extensively studied, accompanied by studies proposing optimal fiber paths for various applications. The authors in [28]–[31] investigated the design of variable stiffness laminates that are enabled through the AFP process. These laminates utilized tow steering to optimize the performance by strategically creating fiber paths that exploit the greatest benefit of the composite material. Variable stiffness design utilizes the guidelines above, however the guidelines are applied locally at each point in a structure to maintain structural integrity. Another manufacturing constraint for variable stiffness laminates is the minimum turning radius of the fibers. This constraint is applied to prevent fiber buckling due to compressive and tensile forces within a tow when steering. Also, uniform load distribution within a structure is rare, leading to locations of a structure with high and low load

requirements. This is accounted for with continuity constraints where ply drops are required to achieve continuity, also referred to as blending. Table 2.1 below, based on the information provided by Beckwith in [21] along with information gathered from Albazzan et al. in [25], summarizes the common design practices for composite structures.

Table 2.1: Typical design practices for design of composite structures [21], [25]

Design Practice	Effect
Employ balanced and symmetric laminates	Minimizes [B] matrix, avoids bending, coupling, warping, and twisting effects
Maximum number of consecutive plies	Prevents delamination and residual stresses
Maximum and minimum ply angle jumps	Decrease inter-laminar stress and obtain dispersed laminates
± 45 -degree surface plies	Increases damage tolerance, buckling load of thin laminates, and protects load carrying plies from impacts
Add fabric as inner and outer layers	Absorbs impact damage and minimizes drilling “breakout”
Pair $+45$ - and -45 -degree plies	Minimizes inter-laminar shear and in-plane shear is carried in tension and compression in the 45 -degree layers
Use larger fraction of \pm plies in shear regions	\pm plies are better at handling shear loads
Minimum steering radius	Prevents fiber buckling and minimize steering defects
Ply drops	Helps with laminate continuity

2.2 LAYUP STRATEGIES

The choice of layup strategy is responsible for determining starting points, reference curves, and coverage across the surface. Each of these choices can enhance or diminish the layup quality. The following will provide a brief description of the available process planning techniques. A detailed review can be found in [32].

2.2.1 REFERENCE CURVES

Before the entire tool surface can be covered with toolpaths, a reference or guide curve is needed. Using various types of reference curves can greatly impact the outcome of the layup. The strategies for creating reference curves are fixed angle, geodesic, and variable angle. A fixed angle strategy creates a curve from a given starting point that has a constant angle from a given axis or direction along the entire surface. The reader can refer to references [33]–[36] for further details.

The geodesic curve method can be used to avoid steering because the curvature along a geodesic path is null. A geodesic is the shortest possible line between two points on a curved surface, resulting in a straight line on a flat plate [37], [38]. The path can be obtained either by specifying a start point and a direction of travel or a start and end point on the surface and the curve will follow the natural path of the surface [32].

Variable angle guide curves vary the fiber orientation along the curve to create variable stiffness laminates [39], [40]. Although there has been recent research in optimizing variable angle paths [25], the calculations and optimizations are more difficult than the other techniques. There are 3 main strategies for defining these reference curves: (1) constant curvature [41]–[43], (2) linear variation [44]–[46], and (3) nonlinear variation

[47]. Each of these strategies uses a slightly different method to define the points and curves for layup trajectories.

2.2.2 COVERAGE STRATEGIES

Various coverage strategies are used to create the course centerlines across the tool surface. There are three strategies that can be used, those being independent curves, offset curves, and shifted curves [32]. The independent curve method uses independently drawn curves to cover the surface. This method is often used on highly complex tool surface's where it is possible to draw the courses staggered, with a constant length, and different directions [35]. Favaloro et al. [34] used this method to create many short courses to limit gaps and overlaps on a conical surface. While this method can limit gaps and overlaps, it is very time consuming and not often used for conventional surfaces.

The offset or parallel curves strategy is the most common one used for path planning [32]. In this strategy adjacent curves are computed from the reference curve to cover the entire surface. The two approaches to define the adjacent curves are a parametrical approach and a mesh approach [30], [35], [36], [48]. The parametrical approach solves a system of equations numerically to define the equations of each successive line. The mesh approach starts from a random reference curve on the mesh surface and uses the Fast Marching Method [49] to propagate this curve, creating the other courses. The advantage computing parallel curves is that they are equidistant which prevents gaps and overlaps between courses. However, when considering a complex surface, the fiber directions of the offset curves can vary from the reference curve. Also, if the initial reference curve has curvature, the neighboring paths will have increased

curvature therefore decreasing the steering radius. If the critical steering radius is exceeded, this will cause further defects.

Lastly, the shifted curve strategy [31], [38], [50], [51] simply shifts the reference curve by applying a translation in its perpendicular direction. The main advantage in using this method is the simplicity in covering the surface with course centerlines. Kim et al. [50] showed that the fiber directions of the shifted paths are not guaranteed on complex surfaces, and an increase in gaps and overlaps can arise.

2.2.3 PATH OPTIMIZATION

The authors in [47], [52]–[54] developed methods to optimize the placement of fiber paths onto the tool surface. Jiang et al. [52] reported a 63.4% to 69% path error reduction using the maximum, mean, and variance of a path error distribution model and optimizing the roller's path. Blom et al. [47] developed a method to optimize course locations based on user requirements of thickness variation in a variable stiffness laminate. The authors in [53], [54] investigated the kinematics of the AFP machine's motion leading to a method of optimization of tool paths based on machine limitation.

2.3 PROCESS PARAMETERS

The parameters used for any specific part are chosen by compromising between layup quality and high layup speeds demanded by industry [55]. Using adequate process parameters is crucial in determining the quality of the layup, and can impact the resulting mechanical properties of the composite part [56], [57]. The main parameters and their effects are summarized in the following.

2.3.1 SPEED

Various layup velocities show alterations in layup quality and required processing parameters [58], [59]. Lower speeds result in longer thermal exposure which results in improved polymer healing up until the applied temperature results in degradation of the material [60]. An increase in layup speed will result in less time that the compaction force and temperature are applied to the material leading to weak cohesive forces [61].

2.3.2 PRESSURE

Compaction pressure is one of the major parameters associated with final part quality [62]. The main concept of applying compaction pressure is to adhere the incoming tows to the substrate and remove voids [63]. The pressure is the critical parameter to develop intimate contact between plies however excessive compaction can lead to material degradation [64]. For the case of thicker laminates, the compaction pressure's influence decreases significantly [65].

2.3.3 TEMPERATURE

Temperature is the main parameter responsible for the development of interlaminar strength since the heat assists in creating the optimal interface between the incoming tows and the substrate [66]. For thermoplastic materials, the applied temperature heats the material above the melting temperature and is then consolidated by applying pressure, and solidifies as it cools [67], [68]. It is imperative not to have a processing temperature significantly above the material's melting temperature because it can lead to material degradation [69], [70]. Further, the temperature parameter can lead to many side effects

that can reduce part quality. For example, deviation in temperatures across the part lead to non-uniform cooling rates resulting in residual stresses and part deformation [71]. The authors in [70], [72] showed that cooling rates are also essential with thermoplastics because it affects the degree of crystallinity, hence effecting the mechanical properties. Other factors such as void dynamics [70], [73], [74], material healing [75], and intimate contact [76] are highly dependent on temperature.

In terms of heating of thermoset materials, the goal is not to reach the melting point but to achieve an appropriate level of tackiness. Appropriate degree of tack is the key mechanism is the formation of most layup defects with thermoset materials and is most influenced by layup temperature [77]–[79]. Higher tack is considered favorable to hold the prepreg on the tool surface as well as ensuring adhesion to subsequent plies [80]. Like thermoplastic heating, excessive temperatures lead to material degradation. Finding the appropriate temperatures for either case is often determined through trial and error [81]. However, tack characterization can provide an adequate starting point for proper applied temperatures [82].

2.3.4 TENSION

Research on fiber tension during the AFP process is limited in the literature. The centralized idea is that tow tension assists in the placement of tows [83]. Excessively high tow tension leads to tow slips due to the tension force overcoming the adherence [84]. Rudberg et al. [85] developed a Modular-Servo-Creel head to address the issue of tension control, leading to increased part quality.

2.3.5 PARAMETER OPTIMIZATION

A large area of research is the optimization of process parameters with the aim to improve manufacturing quality with proper processing parameters. Aized et al. [86] researched the relationship of process parameters and part quality using the response surface method. Through analyzing gas torch temperature, head speed, and compaction force, each parameter was correlated to its effect on process quality. Han et al. [87] developed a multiscale collaborative optimization method for high speed AFP layup in terms of mechanical characteristics of the prepreg tows. Wehbe et al. [88] was able to use numerical techniques to find optimum path curvatures and process parameters for fiber steering on a cylinder.

2.4 AFP DEFECTS

Due to the inherent complexity of the AFP process, defect occurrence is inevitable during the layup. These manufacturing defects can have a significant negative influence on the performance of a given structure [89], [90], thus it is vital to understand the creation and effect of each defect. A majority of defects are a side effect of tool geometry, fiber steering, and material imperfections [91]. All defects can be broken down into 4 main categories: (1) positioning defects, (2) bonding defects, (3) tow defects, and (4) foreign bodies [92]. A comprehensive list of all defect types and their category is given in Table 2.2 below. Harik et al. [91] provides in depth information on the anticipation, existence, significance and progression of each defect, and Brasington et al. [93] accompanies this with visual models of each defect type presented in Table 2.2 that can be 3D printed to aid in learning the geometrical aspects of each defect. The following will provide a discussion

on the four main types of defects (gaps, overlaps, angle deviation, and steering) with images of each gathered from Brasington et al. [93] along with the information gathered from Harik et al. [91].

Table 2.2: List of defect types and their associated category [91]

Defect	Category	Causes	Significance
Gap/ overlap	1	Fiber steering, Layup over complex surfaces	Site for failure initiation, Resin rich areas, Site for wrinkling
Twist	1	Initiated by folding, Rotation during bi-directional layups	Increase/decrease in local thickness
Missing tow	1	Discontinued material feeding, Insufficient tack adhesion	Local thickness variations, Resin rich pockets
Boundary coverage	1	Material cannot perfectly meet at edge of part	Effects shape of part, Failure points if not trimmed
Angle deviation	1	Incorrect roller coverage, Small steering radii	Causes overlaps, Leads to resin rich areas
Wandering tow	1	Unsupported portions of tow between roller and cutter	Leads to gaps and overlaps
Position error	1	Obstruction of tow during feeding, Incorrect machine reference, Machine control issues	Results in gap, Site for failure initiation, More pronounced influence since close to boundary

Table 2.2: List of defect types and their associated category [91]

Defect	Category	Causes	Significance
Fold	2	Tensioner errors, Long or complex tow paths, Steered paths	Substantial influence on local fiber volume fraction, Creates resin rich areas
Pucker	2	Excess tow feeding	Significant loss of strength
Wrinkle	2	Tow placement at small steering radii	Causes gaps and folded tows, Loss of strength
Bridging	2	Too much tow tension, Insufficient tack adhesion	Resin rich areas, Delamination
Loose tow	2	Length of tow is shorter than length between roller and cutters	Results in gaps/overlaps and missing tows
Splice	3	Two tows joined end to end during the slitting process	Local thickness change, Site for failure initiation especially under compressive loads
FOD	4	Resin or fiber fuzz collects on head, Other debris from production area	Improper adherence of next ply

2.4.1 GAPS AND OVERLAPS

The occurrence of gap and overlap defects (Figure 2.1) are the most common in AFP manufacturing. A gap occurs between two adjacent tows when they are not perfectly

laid up, therefore leaving a gap between them. Similarly, an overlap occurs when the two overlap each other. These defects are commonly seen together since when a gap occurs on one side of a tow, an overlap often follow on the other. The most common cause of gaps and overlaps is steering since the tows within a single course will not fit together perfectly. They can also occur naturally due to layup up over a complex surface. A gap defect will result in a resin rich region while an overlap will result in a fiber rich region, both of which will alter the local stiffness properties. Gaps and overlaps are significant since they can become a site for failure initiation and can cause wrinkling in the succeeding layers.

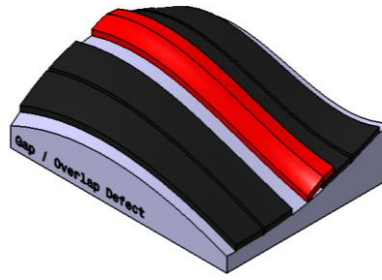


Figure 2.1: CAD representation of a gap and overlap defect

2.4.2 TWIST

A twist defect (Figure 2.2) occurs when a tow is rolled axially 180-degrees onto itself. The tow is then flattened by the compaction roller as it moves across the surface. The geometry of a twist depends on the length of the defect and can be a bow-tie shape for short twists or it can resemble a fold (Section 2.4.8) for longer defects (lengths greater than 5 times the width). The initiation of a twist occurs when a fold grows into a twist, or from friction between the guide holes along a long tow path combined with rotation from the AFP head. Folded tows result in a resin rich region directly next to a fiber rich region, causing a change in thickness and a large effect on local fiber volume fraction.

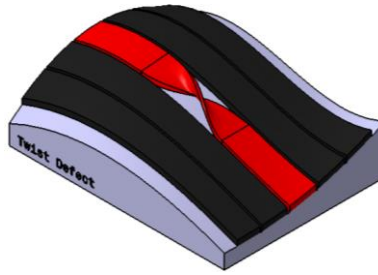


Figure 2.2: CAD representation of a twist defect

2.4.3 MISSING TOW

Missing tow defects (Figure 2.3) are a result of insufficient tack adhesion of an entire tow causing it to fall off the surface, or when the tow is not fed successfully onto the surface. These defects are like gaps and can be considered as a gap with a size equal to a single tow width. The significance of a missing tow is again like a gap in which a resin rich region is created and can result in a point for failure initiation.

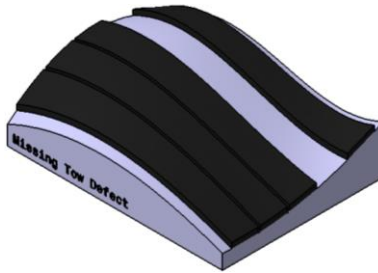


Figure 2.3: CAD representation of a missing tow

2.4.4 BOUNDARY COVERAGE

Often material cannot perfectly line up at the ply boundaries causing a boundary coverage defect (Figure 2.4). Usually this occurs when laying up off-axis orientations such as ± 45 -degree plies and can be at the boundary of any coverage zone whether it is internal or external. This defect results in either an excess or shortage of material at the ply

boundary dependent on the layup strategy used. Boundary coverage can influence the shape of the part since the tows do not line up with the desired part geometry. Trimming of the edges to increase the accuracy can also cause those regions to be more likely to fail.

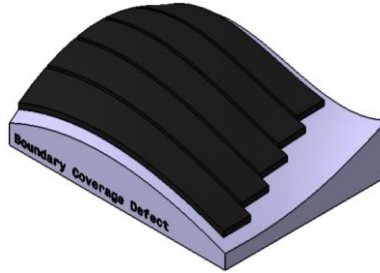


Figure 2.4: CAD representation of a boundary coverage defect

2.4.5 ANGLE DEVIATION

An angle deviation defect (Figure 2.5) is simply when the as-manufactured angle deviates from the as-designed angle. This type of defect can be caused by improper roller coverage or small steering radii. Angle deviation can result in overlaps when successive tows are laid onto the deviated ones. The overlaps lead to an undesired shape and resin rich areas that can cause failure.

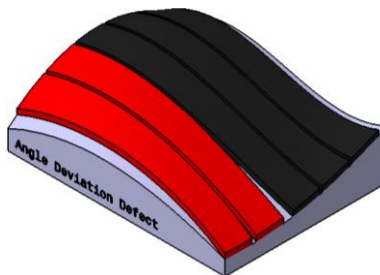


Figure 2.5: CAD representation of an angle deviation defect

2.4.6 WANDERING TOW

The wandering tow defect (Figure 2.6) is like angle deviations in which the tow wanders from the original fiber path. This occurs when the portion of the tow between the roller and cutter is unsupported resulting in the tow wandering. However, the length of the deviation will be limited to the unsupported length. These defects are typically seen at the end of a course and can lead to gaps and overlaps between tows. The resulting defects can result in failure within the laminate.

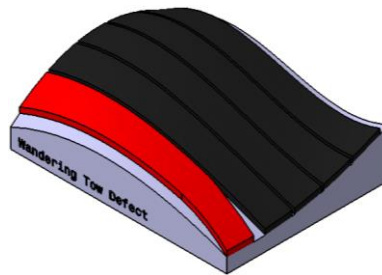


Figure 2.6: CAD representation of a wandering tow

2.4.7 POSITION ERROR

A position error defect (Figure 2.7) occurs when a tow is placed in the wrong location with reference to the beginning or end of the course. As a result, the tow is misaligned with the rest of the tows at the boundary. This type of defect is often caused by an obstruction of the tow path during feeding, incorrect machine reference, or machine control issues. A gap occurs at the location after the tow with the position error. Due to the defect's proximity to the boundary, its effects are expected to be more pronounced due to edge effect failures.

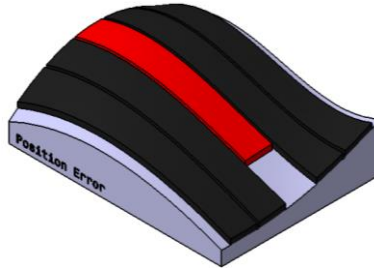


Figure 2.7: CAD representation of a position error defect

2.4.8 FOLD

A fold (Figure 2.8) defect is when a tow folds onto itself in the transverse direction. This results in a gap combined with a doubling of the tow thickness over the folded area. If a fold continues to progress, it can turn into a complete twist of the tow. Folds occur due to tensioner errors, complex unsupported towpaths, or steered paths. This defect can be more serious for cured laminates because of an increase in thickness directly next to a reduced thickness area.

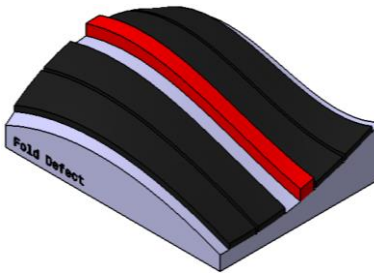


Figure 2.8: CAD representation of a fold

2.4.9 PUCKER

A pucker (Figure 2.9) initiates at the inner radius of a steered tow when the tow lifts from the tool surface. The result is an arch of material that is not adhered to the substrate. Puckers occur due to excess feeding of a tow that accumulates ahead of the

compaction roller and then emerges on the surface. Typically, a pucker is flattened by successive layers or through the debulking process. If the pucker is not flattened it can result in delamination growth between the pucker and the underlying ply which over time can result in complete delamination between layers.

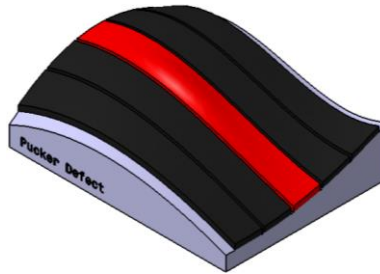


Figure 2.9: CAD representation of a pucker defect

2.4.10 WRINKLE

A wrinkle (Figure 2.10) is a series of puckers that result in a wavy pattern often caused by placing tows at small steering radii. Wrinkling occurs on the inner radius of a steered tow and remains out of plane after further compaction and curing. Since the two edges of a tow are of equal length, the excessive differential length between the two edges when steering causes wrinkles. Wrinkled tows can cause fiber waviness, gaps, and folded tows if they are not flattened by successive layers.

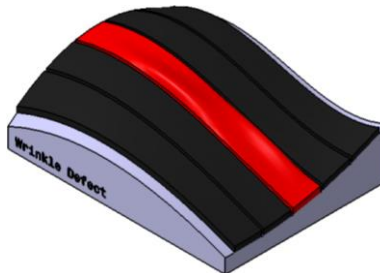


Figure 2.10: CAD representation of a wrinkle

2.4.11 BRIDGING

A bridged tow (Figure 2.11) occurs when a tow does not fully adhere to a concave tool leaving a gap between the tow and the tool surface. The main causes of this type of defect are too much tow tension or insufficient adhesion to a concave tool. Bridging can be prevented by ensuring adequate roller contact or by overfeeding of the tows in concave regions. If the bridged tow is not successfully adhered from sequential passes or debulking, it will result in a resin rich area or possible delamination.

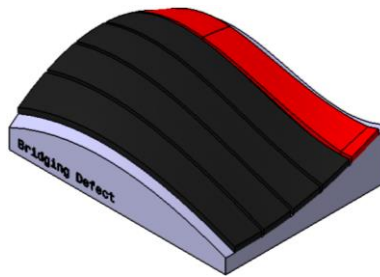


Figure 2.11: CAD representation of bridging

2.4.12 LOOSE TOW

A loose tow (Figure 2.12) occurs when the AFP head tries to place a tow or tows onto the surface without complete and precise control over the placement. This defect can also occur from improper adhesion to the tool surface. A tow is completely loose when the length of a tow is shorter than the length between the cutters and compaction roller. A short length of this kind can be prevented with the setting of a minimum tow length. The loose tow has a chance to cause a significant gap, or a completely missing tow and can result in the effects previously described for those defects.

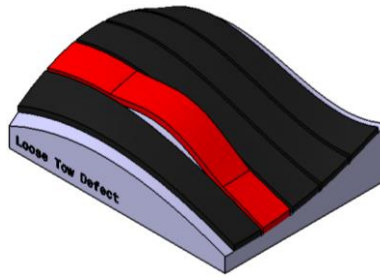


Figure 2.12: CAD representation of a loose tow defect

2.4.13 SPLICE

Splices (Figure 2.13) are a material defect and occur where two tows are joined end-to-end, overlapping 1-3 in., during the slitting process. This results in a portion of the spool being thicker than the rest and are usually marked with white dashes. The occurrence of splices can be limited or eliminated completely by monitoring the spool length and splice location with respect to the size of the part. If the splice is not removed and corrected, it will cause a thickness change and can result in a location for failure initiation.

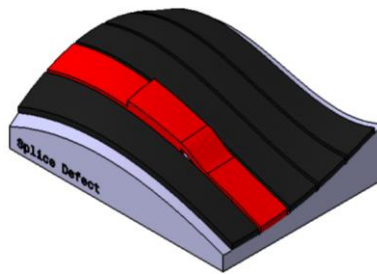


Figure 2.13: CAD representation of a splice

2.4.14 FOREIGN OBJECT DEBRIS

A foreign object debris (FOD) (Figure 2.14) defect occurs when small pieces of either carbon fiber or resin collected within the head and is deposited onto the tool surface, or from debris from the production area. If the FOD is not detected, it will result in a small

excess of either fiber or resin on the ply. This defect can also cause the portion of the next ply above the defect to not adhere properly leading to other types of defects previously described.

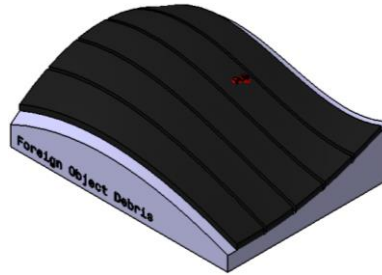


Figure 2.14: CAD representation of FOD

2.5 DESIGN AND PROCESS PLANNING DATA CONNECTION

In the available literature, there is little attempt at integration of design and process planning aspects of AFP structures. The main attempt is provided by Noever et al. with the combination of HyperSizer, Computer Aided Process Planning (CAPP) Module, VCP, and Convergent's COMPRO with a central optimizer to obtain optimum ply boundaries, ply counts, and fiber paths [94], [95]. This work had a higher focus on the performance of the final part based on inputs such as part geometry, internal loads, laminate rules, along with others. This thesis takes the inclusion of design and process planning data from a different perspective. Instead of looking through a design performance lens, this work aims to look through a manufacturing performance lens. This presented approach will account for various design parameter inputs and compare them based how manufacturable they are with various process planning inputs. The output is a different result that does not include the laminate performance directly, however a less manufacturable laminate is assumed to have a lower overall performance.

2.6 DIGITAL TWINS IN THE COMPOSITES INDUSTRY

Rapid developments in technological capabilities in recent years have enabled the marriage between virtual models of complex physical systems and their real-world counterparts. Digital Twin (DT) is a term that embodies this integration of data between the virtual and physical realms. While not at full scale, portions of DT technologies are currently utilized in various industries to enhance existing product lifecycle management (PLM) tools. PLM tools create a system that allows companies and organizations to monitor the progression of a product, beginning from ideation, to manufacture, and ultimately finishing at the product's end of life. In the composites industry today, the activity of PLM is more difficult due to the inherent complexity of a PLM system and the disconnect of information from the phases of PLM. There have been some successes at developing portions of a DT for the composites industry PLM, however no attempts at creating a DT for the entire PLM cycle were found in the available literature [96]–[99]. This gap can be understood through the context of the definition of the term Digital Twin. A general definition of a Digital Twin is given as:

“An integrated, multiphysics, multiscale, probabilistic simulation of an as-built system that uses the best available physical models, sensor updates, product history, etc., to mirror the life of its corresponding twin” [100].

Based on this definition, the foundational components of a DT consist of three things: (1) a physical model, (2) a virtual model, and (3) the data connecting them [101]. The linking between these three features demonstrates that a DT is not a precocious all-in-one model, but a cutting-edge interconnection of data between the virtual and physical domains. The

linking of the lifecycle data into a comprehensive virtual system enables accurate, data backed predictions of the physical product by the DT to enhance significant components of the PLM, such as product design optimization and development of manufacturing systems [102], [103].

CHAPTER 3

DEVELOPMENT OF DATA INTEGRATION TOOLS

3.1 AFP PHASE INTEGRATION TOOL

The main goal of creating the integrated AFP data analysis software, termed neXt Composites (neXtC), is to obtain a single environment where data from each phase of the AFP process can be contained and analyzed. The purpose is not to recreate any current industry tools, but to further analyze the data contained within them to discover correlations or trends that can help improve AFP manufacturing. A new data flow can then be launched, as presented in Section 1.4, where data from each AFP phase can communicate and influence present and future manufacturing trials. This goal also leads to a more refined flow with the ability to streamline and improve the overall process efficiency from part design through the entire manufacturing process. It should be noted that the development of this tool builds on the Computer Aided Process Planning (CAPP) software created by Halbritter [104]. The functions of the CAPP software are detailed in Section 3.4.2.

The initiation of development of such a tool begins with integration of design and process planning data to provide a manufacturability score for the laminate in question. This score utilizes a CAPP ranking (Section 3.4.2) based on anticipated defects generated by VERICUT Composite Programming (VCP). The generated score can then be related back to the design of the tool surface, resulting in a direct comparison of design variables

and manufacturability scores. The following sections will detail the development of the software created to automate the scoring of laminates along with the infrastructure to store and analyze other AFP data. Any functions seen within the software that are not discussed are still under development.

3.2 DATA STRUCTURE

The data structure is the core focus of the neXtC software, as it contains the information which defines the composite structure. Any changes to the data structure must be propagated throughout the interface to ensure informed user actions are performed. This is accomplished through a widget and attribute system. The widget is a general term for the containers displayed on the interface that the user interacts with. A generalized widget system was developed, where a series of signals are connected to each new widget that control the flow of information through a primary controller. Processes and operations can be initiated from each secondary widget when changes to the central data structure are performed. The attribute system enables each of the widgets within the user interface (UI) to have fields that are bound to attributes to classes or instances from the data structure. For example, a user may modify the name of a ply through the property editor, and it will then be updated everywhere else that ply's name is displayed within the UI. The attribute system allows for simple hooks to be created between a widget and the desired attribute. It also allows for additional classes and attributes to be added without interrupting the other aspects of the UI. A breakdown of the data structure within neXtC is provided in Figure 3.1 below.

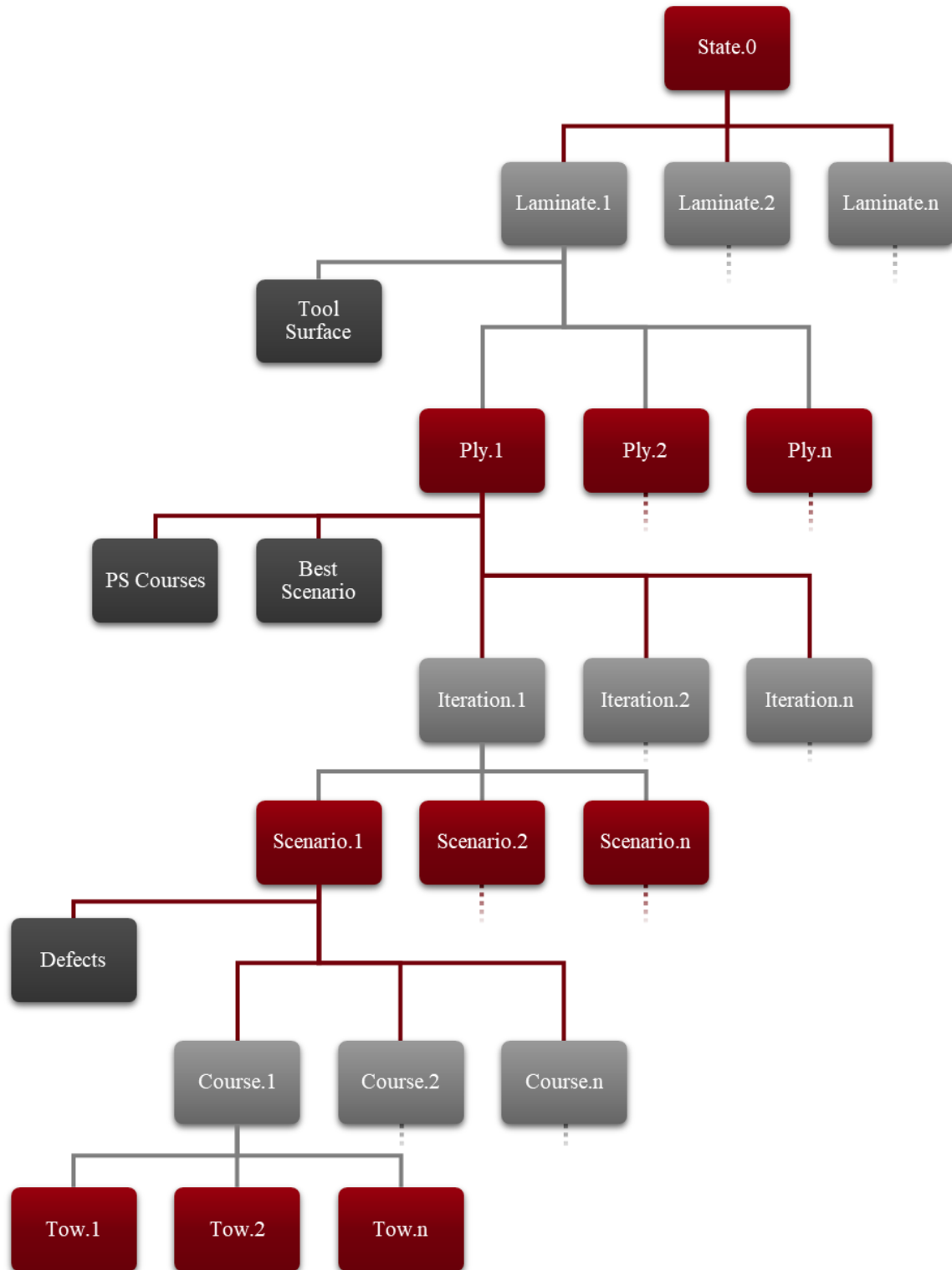


Figure 3.1: Breakdown of the data structure within neXtC

3.3 SOFTWARE INTERFACE

The neXtC software was developed using the Python programming language and an overall view of the layout is provided below in Figure 3.2. The tabs seen along the top are meant to hold the functions needed for use with each phase of the AFP cycle (design, process planning, manufacturing, inspection), along with tabs to define various other types of information for the laminate (specifications, materials). For this thesis, the focus will be on the design, process planning, and manufacturing tabs. Later development will mature other tabs within the software to create an entire PLM workflow.

The software is centered around a computer aided design (CAD) viewer that displays items selected withing the laminate tree and the data associated with them. The left and right docked tabs hold the laminate tree and data analysis tabs respectively. The laminate tree holds data relevant to the laminate in question such as the layup surface, CAPP iterations and scenarios, and inspection data. The series of tabs along the right are employed to analyze process data as it is imported. Here, only the top two tabs (design and process planning) will be used to analyze laminate manufacturability. The latter will detail the various functionalities and the data flow within the software.

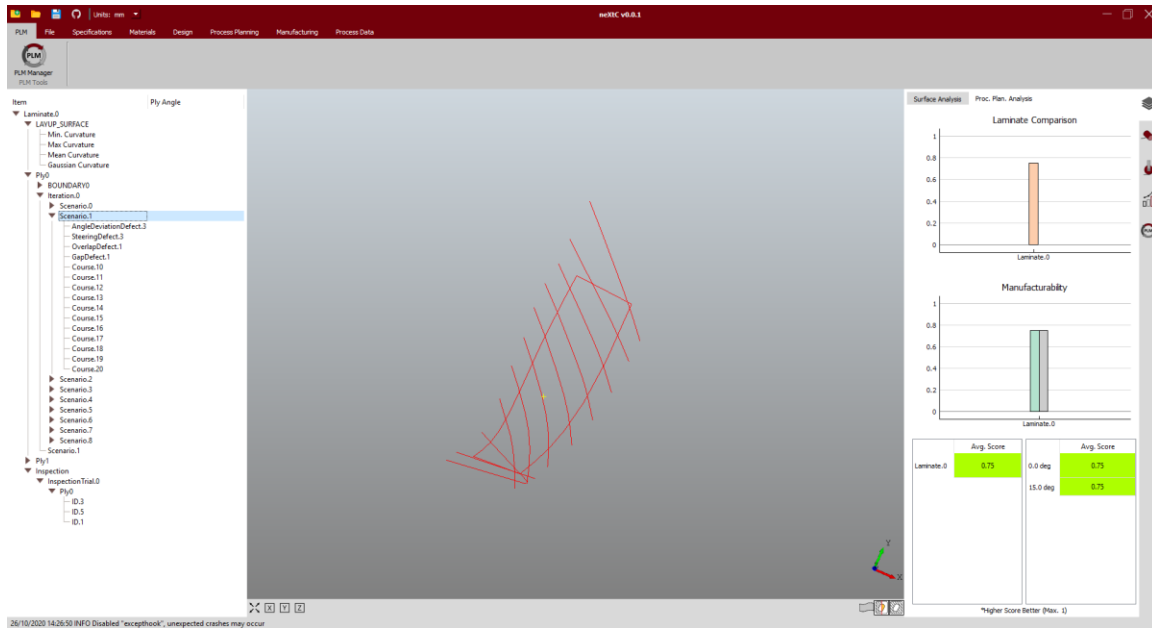


Figure 3.2: neXtC software layout

3.3.1 LAMINATE TREE

Each item that the laminate tree holds is noted below in

Figure 3.3. All data held within neXtC is associated with its corresponding laminate. The current state can then hold multiple laminates for comparison of data between each one if desired. Contained within a laminate is a layup surface which is imported from a step file or, in the case of basic geometries, can be generated within the software. To import as a step file, the naming convention for the layup surface within the chosen CAD package must contain “layup_surface” and each boundary must contain “boundary”. Functions then allow the user to examine the curvature of the surface, which is held as children of the layup surface.

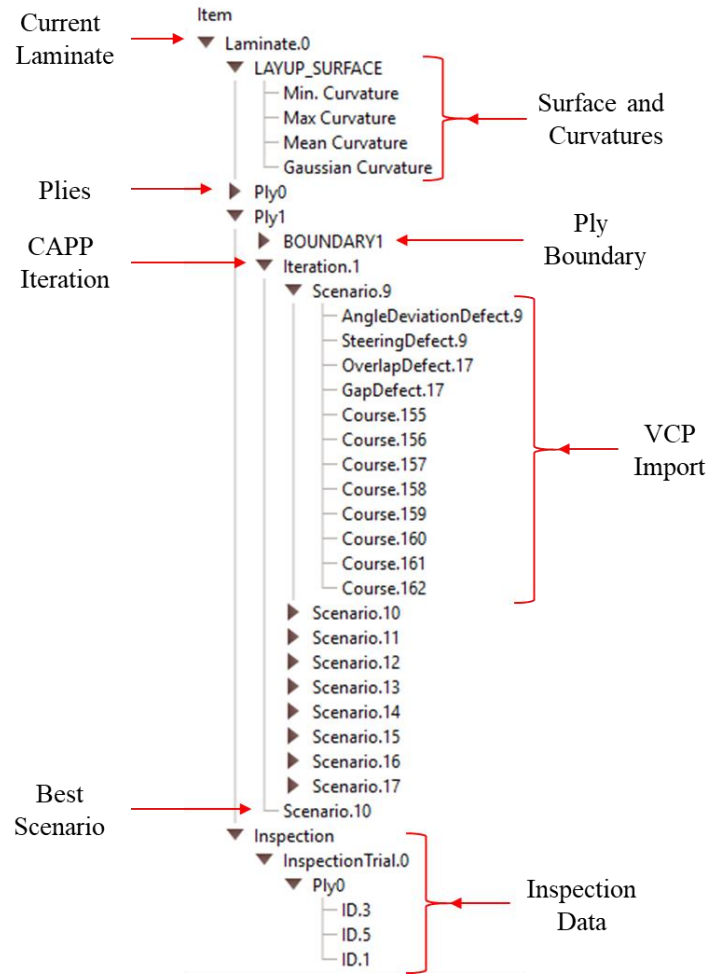


Figure 3.3: Description of the laminate tree

Next, the laminate tree contains the plies for each laminate. The plies are either defined automatically with the imported boundaries, or they can be manually added to the tool surface. The first branch of each ply contains the ply boundary for the associated ply. The branches of the boundary hold the split surface, mesh surface, and heat kernel signature (HKS) surface generated by the CAPP functionalities.

Underneath the boundary branch is each iteration generated by the CAPP functionality (a single iteration in this case). Each iteration contains up to 9 scenarios, or

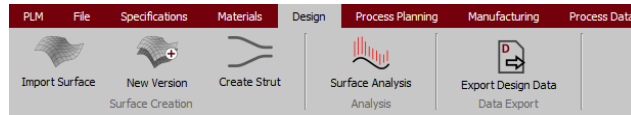
starting points, that are created in a 3x3 array of a set width. After performing a VCP analysis, defect data for angle deviations, steering, overlaps, and gaps along with the courses for each scenario are stored. Each ply keeps track of the best scenario when the user scores the plies.

Lastly, the inspection branch contains inspection trials that contain the various defect types found for each ply. This data is generated from the ACSIS inspection system and then analyzed through ML algorithms developed by Sacco et al. The results are then converted into an xml file and imported into neXtC for comparison between anticipated and actual defects.

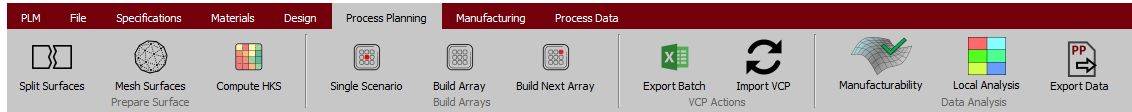
The following sections will describe the functions used within neXtC to import, create, analyze, or export the necessary data.

3.3.2 OPERATION INTERFACES

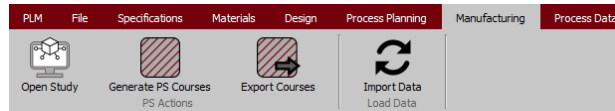
The buttons that control the functionalities within the software are contained within tabs along the top of the interface. These tabs are split into categories based on the phases of the AFP process. The design tab (Figure 3.4a) contains buttons for surface creation, surface analysis, and data exporting. The process planning tab (Figure 3.4b) contains functions relating to the CAPP process. These consists of surface preparation, building scenario arrays, VCP actions, manufacturability calculations, and data exporting. The manufacturing tab (Figure 3.4c) currently holds actions to open a digital twin study inside PS, exporting courses from neXtC to PS, and importing data generated externally.



(a)



(b)



(c)

Figure 3.4: Buttons with the (a) design, (b) process planning, and (c) manufacturing tabs

The data analysis viewers are contained within the toolbar on the right side of the screen. This toolbar contains tabs to view the data from each AFP phase. The design data tab (Figure 3.5a) contains data relating to surface manufacturability analysis and overall manufacturability of the current design. The process planning data tab (Figure 3.5b) contains data related to layup strategy definitions, anticipated defects, ranking strategies, and scenario scores.

The user also has the option to adjust the views within the interface. The buttons presented in Figure 3.6a (from left to right) allow the user to reset the zoom, view the x-plane, view the y-plane, and view the z-plane. The viewer options shown in Figure 3.6b allow the user to control the viewability of the tool surface, split surfaces, and ply boundary.

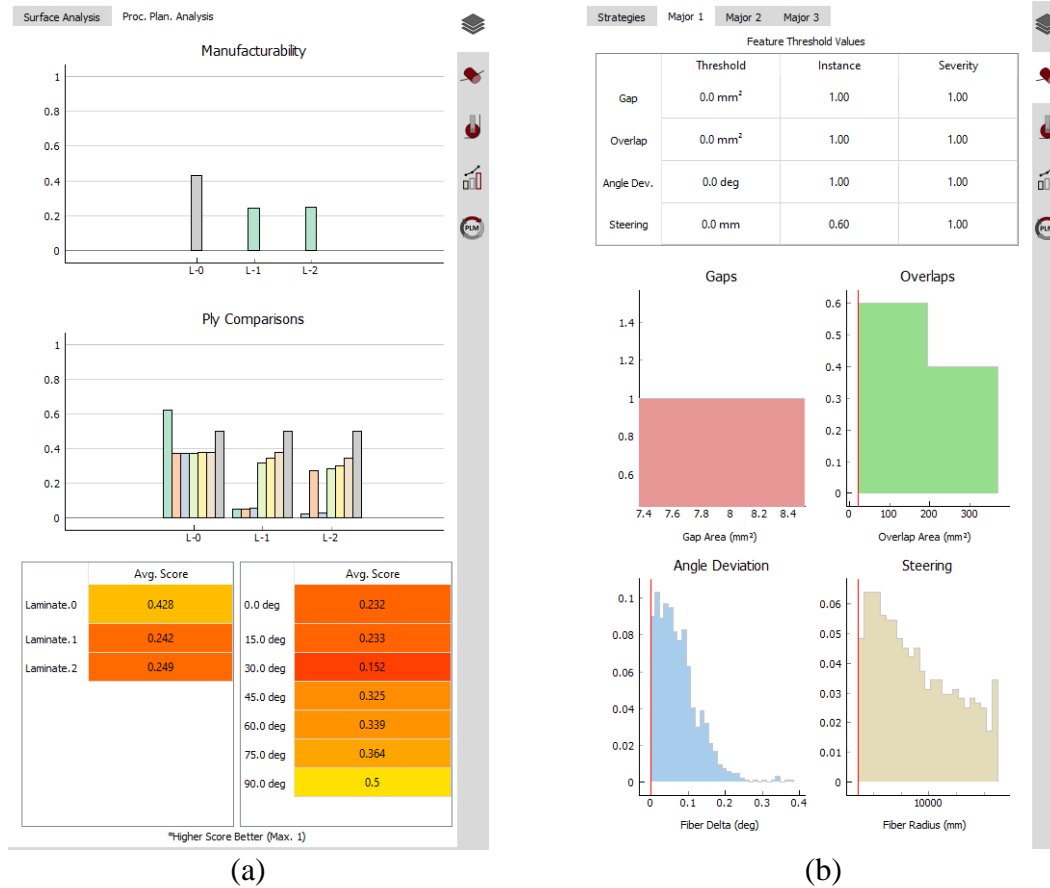


Figure 3.5: Data analysis viewers for (a) design and (b) process planning data



Figure 3.6: Interface viewing related buttons

The buttons along the top of the software are shown in Figure 3.7. These buttons allow the user to create a new file, open a file, and save a file. The fourth button from the left launches the wiki which provides a tutorial on how to use the software. The units can also be changed in this region to switch between millimeters and inches.



Figure 3.7: Buttons to control project data

3.4 FUNCTIONALITIES

3.4.1 DESIGN FUNCTIONALITIES

All actions linked to creating or analyzing the tool surface are contained within the design tab (Figure 3.4a). Note that outside of basic geometries, the tool surface must be generated via an external CAD package. Currently, the workflow begins with either importing or internally creating a tool surface. As mentioned previously, a tool surface and its plies can be imported via a step file with the appropriate naming convention of the tool surface and boundaries. This style of importing allows for the user to use any CAD package to generate the necessary geometries since most packages will have the ability to export as a step file. When importing, the dialog box shown in Figure 3.8 is presented to the user. Any CAD entity that is label appropriately will be shown here. The user can add and subtract plies and choose the entities to associate with each ply to create the stacking sequence for the laminate. The design tab also allows the user to import a new version of the laminate in question. The new laminate does not have to be related to the previous one, however the manufacturability scores of each will be automatically compared.

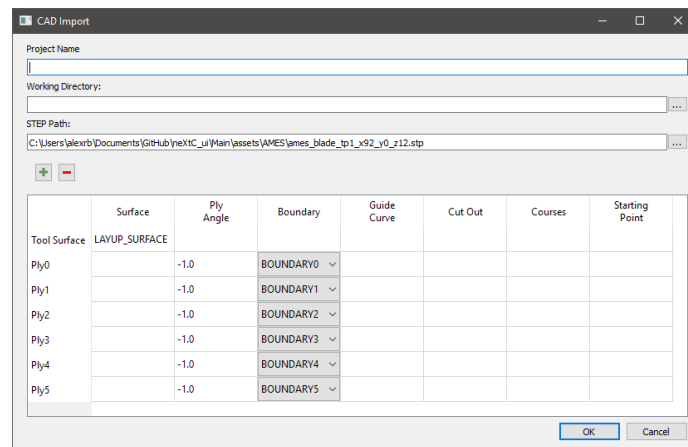


Figure 3.8: Surface import dialog box

For basic surface geometries, the tool surface can be created within neXtC for rapid design iterations. Previous experimentation required the creation of a strut geometry. Utilizing the strut creation button, the user can define the geometrical parameters and number of plies. The input options are shown below in Figure 3.9. These inputs are then used to automatically create the strut surface, boundaries, and associated plies. Future developments will build on this functionality with the addition of a wider selection of geometric options.

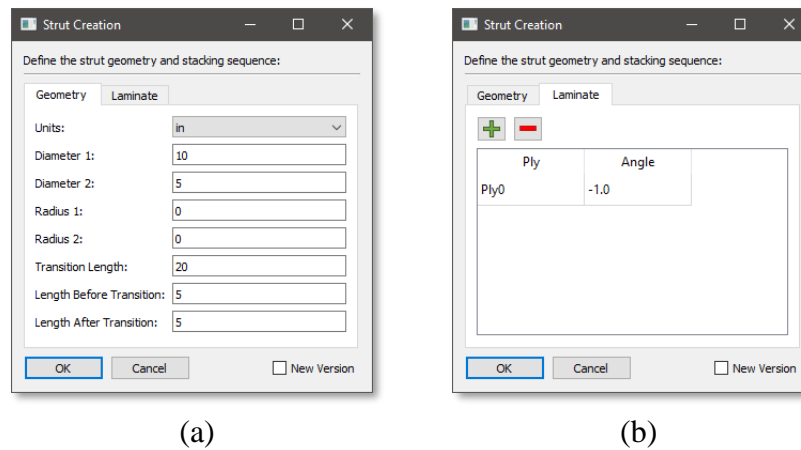


Figure 3.9: User input boxes for creating (a) strut geometry and (b) plies

At this point the user can also define design parameters that will be used to analyze manufacturability. Each parameter will be correlated to the manufacturability of each ply and the entire laminate. The imported or internally created tool surface can be analyzed through Gaussian curvature calculations (Figure 3.10). The curvature values are combined with defect data to analyze correlations of defect occurrence with surface curvature and design parameters. This data can then be utilized to refine the tool surface along with influencing future designs. The curvature values are also used to provide an initial

manufacturability approximation of the tool surface. All data generated with this tab can also be exported to a csv file for further analysis externally.

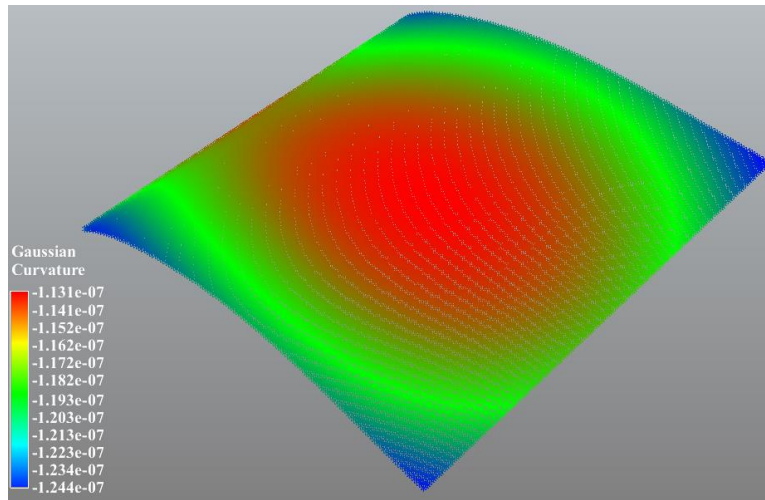


Figure 3.10: Example of tool surface curvature analysis

3.4.2 PROCESS PLANNING FUNCTIONALITIES

Once the tool surface has been imported and any desired surface analysis is completed, the user can proceed with the CAPP process. The process leverages the well-developed VCP functionalities. All necessary functions are connected to the buttons in the process planning tab (Figure 3.4b).

The process begins with splitting the tool surface at each ply boundary to isolate the surface inside (Figure 3.11a). The inner surface is then meshed with a user specified density. Using the mesh surface, a heat kernel signature (HKS) analysis is performed (Figure 3.11b). This calculation basically heats up the part and sees where the heat is last to dissipate from. Each of these processes are classified as surface preparation and can be done with the first 3 buttons in the process planning tab.

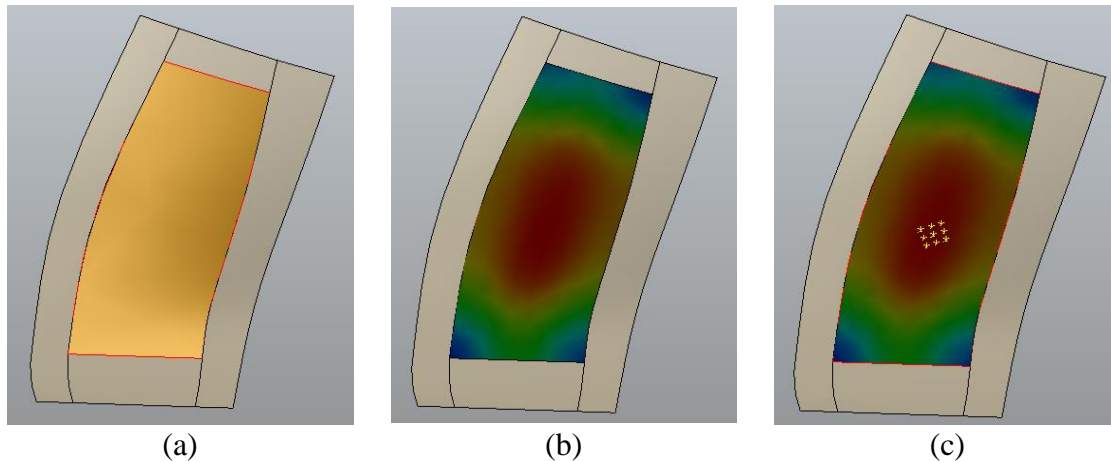


Figure 3.11: Example of (a) surface splitting, (b) meshing and HKS, and (c) scenario creation in the CAPP process

Next, the user can select an option to build the starting point arrays. Before building scenarios, the user can select which layup strategies to use from those available in VCP (Figure 3.12). A scenario will be built for each strategy selected.

Path geometries

☐ Rosette rule

☐ Natural

☐ Limited steering

☐ Parallel

☐ Rosette / parallel

☐ Natural / parallel 1

☐ Natural / parallel 2

☐ Natural / flared

Figure 3.12: User selection of layup strategies

The user can either build a single starting point for each strategy at the max HKS value or build a 3x3 matrix for each with the center point at the max HKS value (Figure 3.11c). Building a single scenario is used for rapid analysis of manufacturability, whereas the matrix of points is utilized for optimization of the starting point. The third button in the build arrays section of the tab is used to build another 3x3 array of points centered on the

best scenario extracted through the scoring process. This iteration process can be done until a point is converged on, or until the user is satisfied the manufacturability score.

The generated scenarios can then be exported to a template that can be imported directly into VCP. With the imported data, VCP generates the courses and provides an anticipated defect analysis. This analysis contains data associated with gap, overlap, angle deviation, and steering defects. The data generated by VCP is then imported back into neXtC and is visually available through the CAD viewer and through histograms (Figure 3.13).

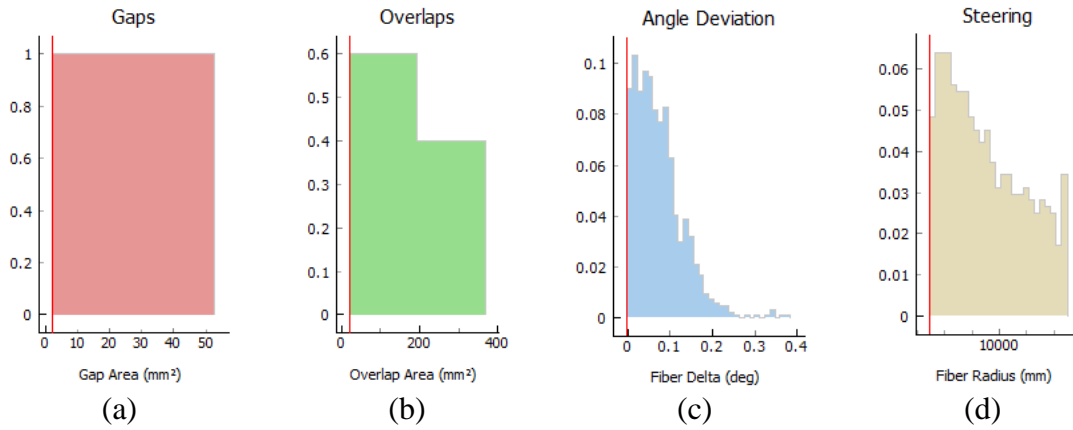


Figure 3.13: Histogram representation of defect data

To analyze the imported defect data, the user must first input some values. The first values to input are threshold values for gap area, overlap area, angle deviation allowance, and steering radius allowance. The input values can then be used to compute instances and severity of each defect using the Equation 3.4.1 and 3.4.2 below.

$$Instance = \frac{\# Unacceptable}{\# Total} \quad 3.4.1$$

$$Severity = \frac{Accumulated\ defect\ above\ threshold}{Total\ sum\ of\ defects} \quad 3.4.2$$

The results are then tabulated and presented within the software as shown in Figure 3.14.

An instance and severity value of 1 corresponds to all the defects being above the acceptability limit given by the user.


Feature Threshold Values

	Threshold	Instance	Severity
Gap	0.0 mm ²	0.00	0.00
Overlap	0.0 mm ²	0.00	0.00
Angle Dev.	0.0 deg	0.00	0.00
Steering	0.0 mm	0.00	0.00

Figure 3.14: Feature threshold value chart

To calculate a single score that combines instance and severity of each defect, an analytic hierarchy process (AHP) matrix is used (Figure 3.15). The goal of this matrix is to rank each set of defects based on their importance. The user can change the values within the AHP matrix to put priority on certain defects. This matrix is then converted into rankings that are used to compute the score of each scenario.

	Gap Instances	Gap Severity	Overlap Instances	Overlap Severity	Angle Dev. Instances	Angle Dev. Severity	Steering Instances	Steering Severity
Gap Instances	1.0	1.0	1.0	1.0	1.0	1.0	1.0	1.0
Gap Severity	1.0	1.0	1.0	1.0	1.0	1.0	1.0	1.0
Overlap Instances	1.0	1.0	1.0	1.0	1.0	1.0	1.0	1.0
Overlap Severity	1.0	1.0	1.0	1.0	1.0	1.0	1.0	1.0
Angle Dev. Instances	1.0	1.0	1.0	1.0	1.0	1.0	1.0	1.0
Angle Dev. Severity	1.0	1.0	1.0	1.0	1.0	1.0	1.0	1.0
Steering Instances	1.0	1.0	1.0	1.0	1.0	1.0	1.0	1.0
Steering Severity	1.0	1.0	1.0	1.0	1.0	1.0	1.0	1.0



	Rankings
Gap Instances	0.12
Gap Severity	0.12
Overlap Instances	0.12
Overlap Severity	0.12
Angle Deviation Instances	0.12
Angle Deviation Severity	0.12
Steering Instances	0.12
Steering Severity	0.12

Figure 3.15: AHP matrix and rankings

The individual scenario scores are computed using Equation 3.4.3. Here the ranking weights are those computed through the AHP matrix, and the measurement values are from the instance and severity calculations. The scores for all scenarios can be automatically computed with the manufacturability button. This also finds the best score for each ply and stores it for further manufacturability calculations.

$$Score = \sum Ranking\ Weight * Measurement\ Value \quad 3.4.3$$

The final manufacturability calculation for the entire laminate is computed using Equation 3.4.4. In this equation, the ply score is the maximum score from all scenarios in the associated ply. Through future manufacturing trials, a threshold manufacturability value will be found to define if it is acceptable to continue with manufacturing or if further refinement is necessary.

$$Manufacturability = \sum_{n=1}^{\#plies} Score_n * Ply\ Area_n / \sum_{m=1}^{\#plies} Ply\ Area_m \quad 3.4.4$$

A detailed presentation of the functions presented here can be found in [104].

3.4.3 MANUFACTURING FUNCTIONALITIES

The manufacturing functionalities within neXtC are still in an adolescent stage. However, a few important actions have been developed. The first of these is the ability to open a Siemens Tecnomatix Process Simulate Process Simulate (PS) study from within the neXtC interface. This action creates the initiation of data communication with another software. The user can also generate and export the courses from chosen scenarios. The user dialog for generating the courses is shown in Figure 3.16a. In this dialog, the user can

select scenarios for which courses will be generated. In the case of multiple scenarios for a single ply, the scenario with the best manufacturability score will be highlighted.

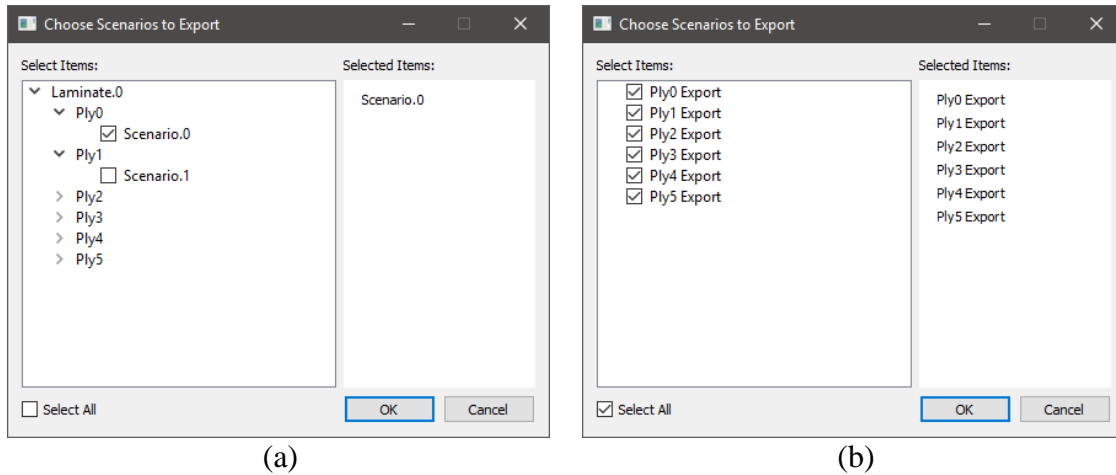


Figure 3.16: User interface to select scenarios to export

Upon generation, the roll-in and roll-out are added to the course centerlines and points are created where tows begin and end (Figure 3.17). These points are labeled with a tow mask that tells PS where each tow starts and stops along the course. This will allow PS to be able to simulate actual layup, as well as directly program an AFP machine. The file is then saved as a step file that can be imported into PS.

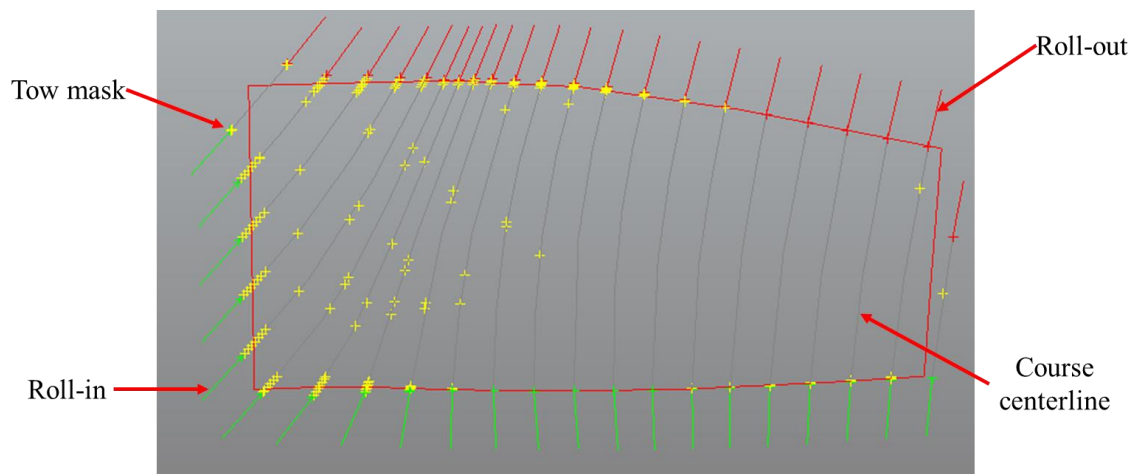


Figure 3.17: Description of courses for PS

3.5 MANUFACTURABILITY ANALYSIS

Using the manufacturability values calculated with the process planning functionalities of neXtC, the laminate and ply scores of the designed surface can be compared. The software does this automatically when the manufacturability button in the process planning tab is clicked. The analysis is then presented to the user graphically (Figure 3.18) and numerically (Figure 3.19).

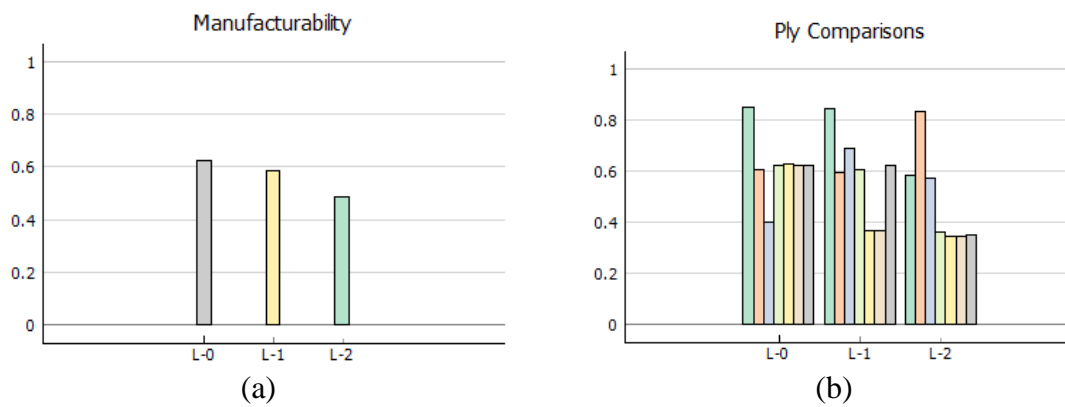


Figure 3.18: Graphical comparison of manufacturability of (a) laminates and (b) plies

The graphical presentation provides a quick look into the performance of each laminate and ply. However, the numerical tabulated results provide a clearer picture of the exact manufacturability values, and how they compare with each other.

	Avg. Score
Laminate.0	0.622
Laminate.1	0.584
Laminate.2	0.484

(a)

	Avg. Score
0.0 deg	0.759
15.0 deg	0.678
30.0 deg	0.553
45.0 deg	0.529
60.0 deg	0.448
75.0 deg	0.444
90.0 deg	0.532

(b)

Figure 3.19: Numerical comparison of manufacturing of (a) laminates and (b) plies

3.5.1 LOCALIZED ANALYSIS

With the imported defects and the calculated surface curvatures, the manufacturability can be further analyzed locally. This is done by splitting the surface using a grid with user specified segments in each direction. Using the same grid, the defects are also split into the various boxes. An example of this splitting is shown below in Figure 3.20.

Local calculations within each box are then used to demonstrate what portions of the surface present manufacturability issues. The curvature in each box is found by isolating the coordinates within that box, finding the curvatures that correspond to those coordinates, and then averaging the found curvatures. This same method is also used to calculate the steering and angle deviation defects in each box. A similar method is used for the overlap and gap defects. Each defect polygon within a certain box is isolated, and the area is calculated. This area is then compared with the overall area of that box to find how much of the box is covered by defects. The calculated values for each case are then associated with red, green, blue (RGB) colors where blue is the lowest value and red is the highest.

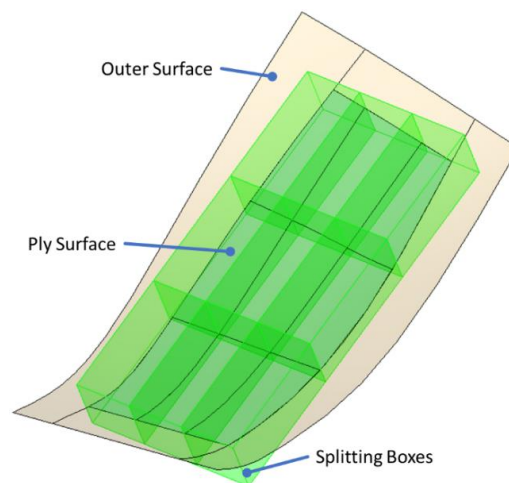


Figure 3.20: Splitting of the surface and defects

Utilizing the localized defects, a local manufacturability score can be calculated. This starts with normalizing each defect area found above to a value between 0 and 1. Normalization is done with respect to the maximum value of each individual defect, meaning that all gap values are normalized with respect to each other and so on. Note that 1 minus the normalized steering values are used since a higher steering radius is preferred. An exception to this rule is a steering value of 0, in which this value is directly used since no steering is present. Using the normalized values within each box, the local manufacturability is calculated with Equation 3.5.1 below.

$$Score_n = 1 - \frac{\sum_{m=1}^4 Defect Area_{n,m}}{4} \quad 3.5.1$$

Here, n corresponds to the current split surface, m represents each normalized defect value to be added (1. Gaps, 2. Overlaps, 3. Angle Deviations, 4. Steering), and $Defect Area_{n,m}$ represents the defects of the corresponding type in the current region. The total of the summation is then divided by 4 since this is the maximum possible value. 1 minus this value then gives the manufacturability score, where 1 is the best score and 0 is the lowest. The surface within each box is then plotted with the corresponding colors as shown in Figure 3.21.. This can be used to visualize local values of gaps, overlaps, angle deviation, steering, and manufacturability. Note that the localized calculations do not factor in any threshold values like the complete ply and laminate analyses do. This is purposeful and is done to provide a complete understanding of all defects that are present. Comparisons utilizing the localized and non-localized results provides a comprehensive understanding of the defect type, size, and location.

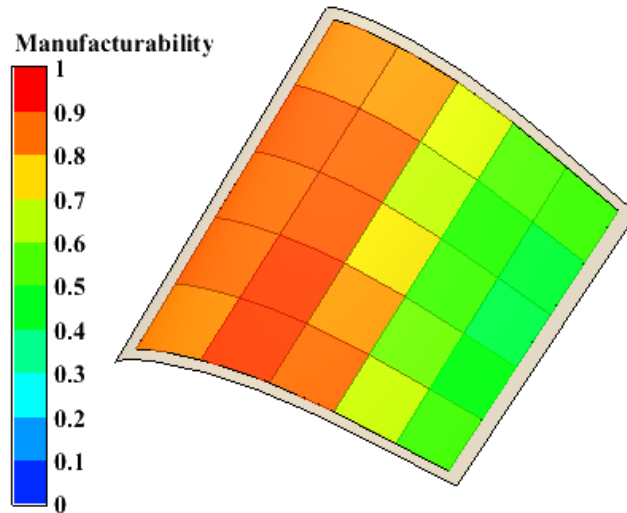


Figure 3.21: Example of the manufacturability section analysis of the tool surface

3.5.2 LAMINATE COMPARISON

Further correlations are then found using correlation matrices such as the one presented in Figure 3.22. The user can either view an entire correlation matrix with all variables present or choose certain parameters to isolate. In these matrices, a value of 1 indicates a perfectly positive linear correlation between two variables, -1 indicates a perfectly negative linear correlation between two variables, and 0 indicates no correlation between two variables. The correlation matrix is also a symmetric matrix with the diagonal values always being 1 since it is a direct comparison between the same variables. The matrix values provide the user with immediate knowledge on what variables of their design are leading to manufacturability issues without having to analyze each one separately.

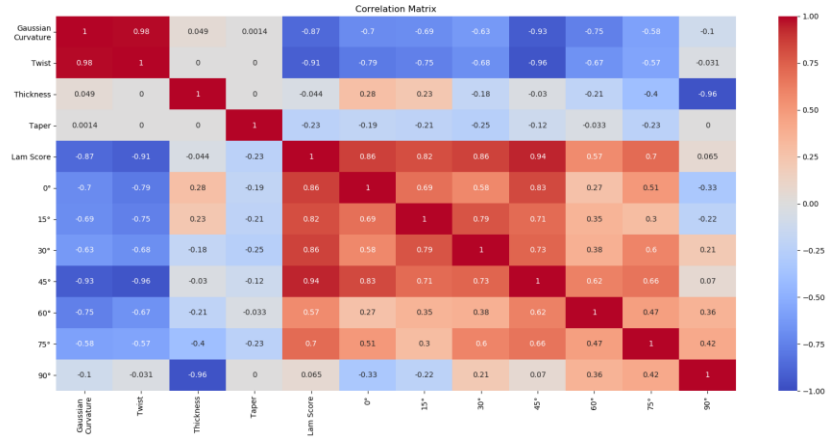


Figure 3.22: Manufacturability correlation matrix

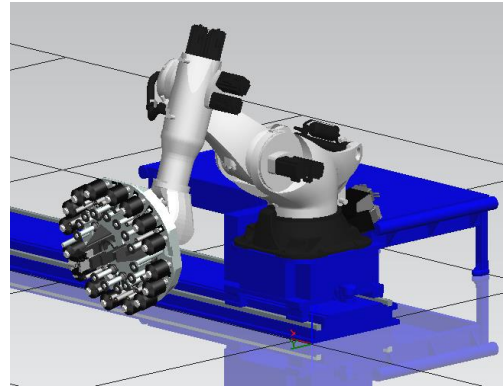
3.6 DIGITAL TWIN CREATION

An initial creation of a DT for the ISAAC AFP cell at NASA LaRC is developed. This AFP machine is a robotic arm type supplied by EI with a linear and rotary external axis. The software chosen to develop the digital twin is PS. This tool was chosen due to its robustness, simulation accuracy, and several data reporting tools. PS provides tools such as 3D simulation and editing, collision detection, joint monitoring, and data communication. The data gained from the DT is expected to flow between all phases of the AFP process to improve the overall lifecycle. Note that several DT concepts developed by the neXt research team at the McNAIR Center are directly applied here [105].

Creation of the DT started with importing existing CAD models into PS. These models are provided by the team at NASA LaRC. Figure 3.23 presents a comparison between the physical model and the digital model. Due to restrictions (COVID), the accuracy of the model could not be exactly determined. However, dimensions of the cell were provided, and the model was matched to these dimensions. The items included in the DT consist of the AFP machine, linear rail, rotary, and the layup table.



(a)



(b)

Figure 3.23: Comparison of the (a) physical and (b) digital ISAAC AFP machine

The elements of the cells are associated with “links” that describe how each component moves and how groups of components move together as a single unit in context of the kinematic tree shown in Figure 3.24. Each link is associated with a joint that can be either prismatic or rotational. The limitations on joint positions, velocities, and accelerations are specified within the KUKA robot file.

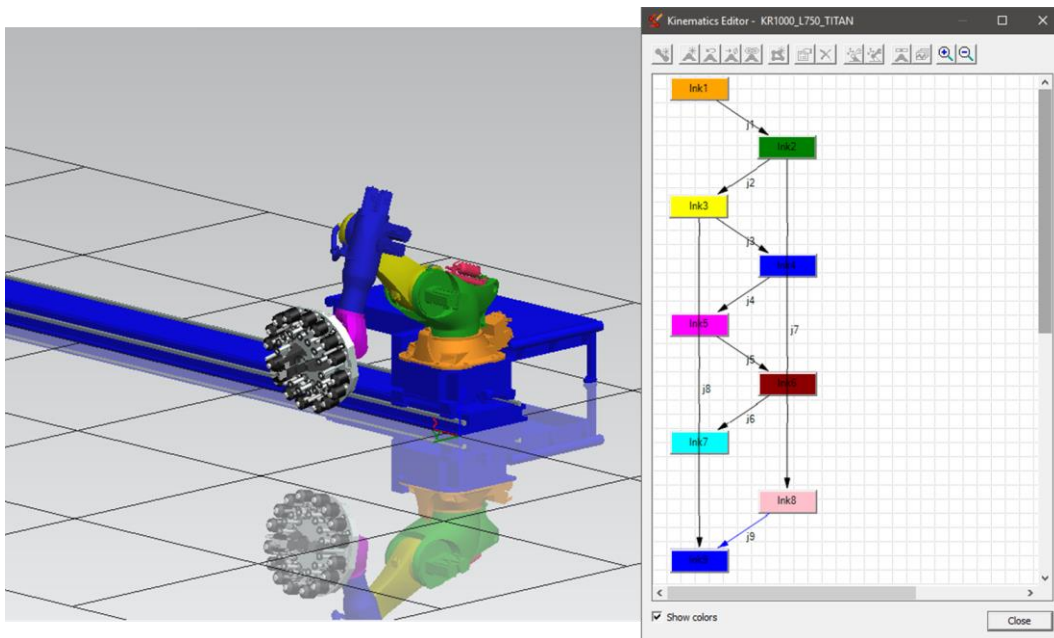


Figure 3.24: Kinematic setup of the AFP machine

The AFP head is created as a tool that can be attached to the robot. It is anticipated that future developments will create the ability to utilize multiple AFP heads in a single simulation. This will enable the simulation and tracking of head changes, along with being able to use other types of heads such as a tape laying head. Frames are then defined at the tool center point (TCP) of the robot, which in the case of the AFP head corresponds to the nip point of the roller (Figure 3.25). Simulations can now be performed from courses created within PS or exported from neXtC.

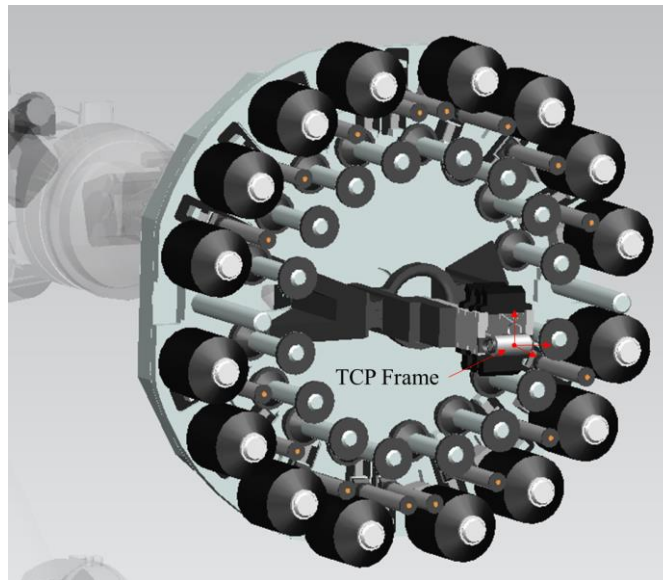


Figure 3.25: TCP location on the AFP head

3.7 SUMMARY

The data integration software, titled neXtC incorporates a class-based data structure that holds the necessary data from each AFP phase. The stored data can then be viewed and analyzed through the UI. The presented functionalities include actions related to design, process planning, and manufacturing. Also, the creation of a DT of the ISAAC AFP

cell at NASA LaRC is developed. The DT provides the capabilities to link the data from the various phases into a virtual environment that can be used for simulations and analysis.

CHAPTER 4

EXPERIMENTAL VALIDATION PLAN

4.1 TEST MATRICES

Experimentation consisted of a parametric study of a generic strut and airfoil shape to investigate the manufacturability of various shapes based on their design parameters. The goal of the experiment is to connect the process planning data with the designed surface to generate an initial manufacturability approximation. The latter will detail the test matrix for the experiments.

4.2 STRUT EXPERIMENTS

Experimentation consisted of a parametric study of a general strut geometry to investigate its manufacturability based on various design inputs and to choose an optimal shape. The design parameters are set to be the transitions length and the radius at the beginning and end of the transition zone. Three different transition zone lengths (7 in., 14 in., 22 in.) and three radii values (0 in., 1 in., 2 in.) are used resulting in the 9 design variations shown in Figure 4.1.

The trial IDs that will be used to differentiate between each trial are presented in Table 4.1. For each ID, the first number represents the trial number, and the second number represents the number of tows used in the respective trial. This table also provides each of the design variables used for each trial. All trials utilized tows with a width of 0.25 in. Also

note that all trials use the rosette rule layup strategy due to unsuccessful course generation with other strategies in VCP.

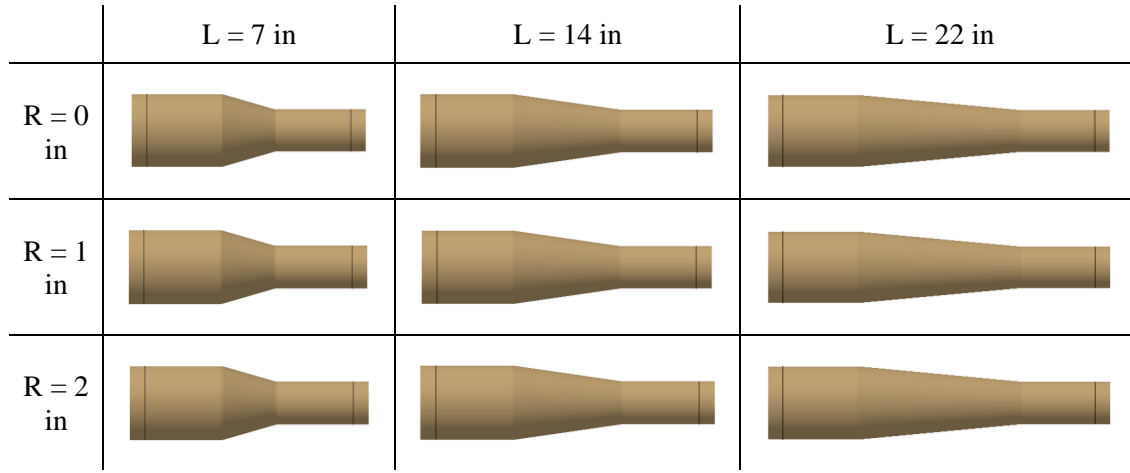


Figure 4.1: Graphical representation of the strut trials matrix

Table 4.1: Description of each variable for the strut trials

Trial	D1 (in.)	D2 (in.)	L (in.)	R1 (in.)	R2 (in.)
1-4	4.75	2.75	7	0	0
2-4	4.75	2.75	14	0	0
3-4	4.75	2.75	22	0	0
4-4	4.75	2.75	7	1	1
5-4	4.75	2.75	14	1	1
6-4	4.75	2.75	22	1	1
7-4	4.75	2.75	7	2	2
8-4	4.75	2.75	14	2	2
9-4	4.75	2.75	22	2	2
1-2	4.75	2.75	7	0	0
2-2	4.75	2.75	14	0	0
3-2	4.75	2.75	22	0	0
4-2	4.75	2.75	7	1	1
5-2	4.75	2.75	14	1	1
6-2	4.75	2.75	22	1	1
7-2	4.75	2.75	7	2	2
8-2	4.75	2.75	14	2	2
9-2	4.75	2.75	22	2	2

*Rosette Rule used; other strategies generated errors in VCP

4.3 AIRFOIL EXPERIMENTS

A parametric study is carried out for a NACA 63-415 airfoil. In this case, the design parameters are set to be chord length (0.5m, 0.75m, 1m), twist angle (10° , 20° , 30°), thickness (50%, 100%, 150%), and taper (75%, 50%, 25%). Each of the thickness values is the percentage based on the base geometry of the airfoil. The taper percentage is the smaller chord length divided by the initial chord length. For example, a 75% taper means that the one end of the airfoil is 75% of the other end. For all cases the span of the airfoil is set to be 1 meter. To examine the combinations of these design parameters, 3 test matrices were used. The initial experimentation consisted of preliminary analysis of the generic airfoil shape with various thickness and chord length values. A graphic representation of the airfoil with the parameters chord length and thickness is presented in Figure 4.2.

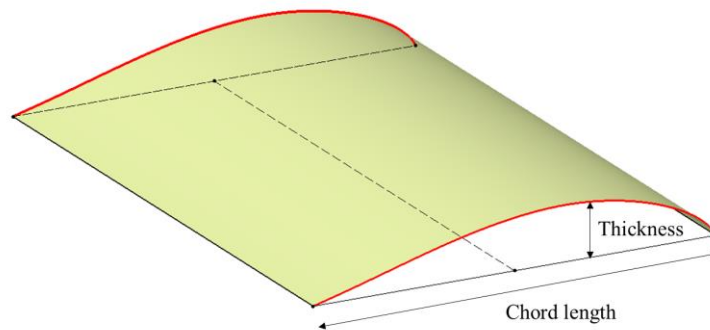


Figure 4.2: Airfoil shape for examining thickness vs. chord length

Utilizing combinations of the chord length and thickness values presented above, the test matrix in Table 4.2 was created. This generates a total of 9 variations to be analyzed and compared.

Table 4.2: Test matrix for examining chord length and thickness of the airfoil

ID	Chord Length (m)	Thickness (%)
0.5-50	0.5	50
0.5-100	0.5	100
0.5-150	0.5	150
1.0-50	1.0	50
1.0-100	1.0	100
1.0-150	1.0	150
1.5-50	1.5	50
1.5-100	1.5	100
1.5-150	1.5	150

The next series of experiments consisted of combining the twist and taper values. The effect of these values on the surface is shown in Figure 4.3. The initial airfoil surface is translated 1m as mentioned above to produce the span of the airfoil. The translated airfoil is then rotated by the twist angle, with the rotation axis being the dashed line connecting the two airfoil shapes. The rotated airfoil is then scaled with reference to the midpoint of the chord line by the specified taper value.

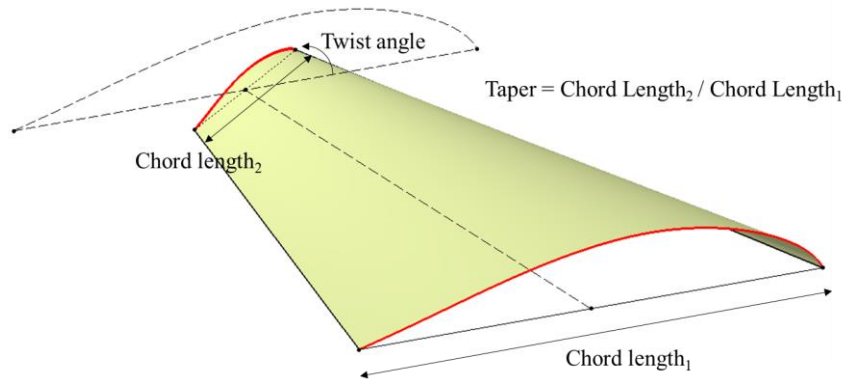


Figure 4.3: Airfoil shape with variations in twist and taper

Using the 3 twist angles and 3 taper percentages, another test matrix of 9 variations is generated and provided in Table 4.3.

Table 4.3: Test matrix for examining twist and taper of the airfoil

ID	Twist Angle (°)	Taper Percentage (%)	Chord Length₁ (m)
10-75	10	75	1.0
10-50	10	50	1.0
10-25	10	25	1.0
20-75	20	75	1.0
20-50	20	50	1.0
20-25	20	25	1.0
30-75	30	75	1.0
30-50	30	50	1.0
30-25	30	25	1.0

The final set of experiments for the airfoil parametric study examines the combination of twist angle and airfoil thickness. As previously mentioned, the initial airfoil shape is translated by 1m to create the span, and then the translated airfoil shape is rotated by the twist angle to produce the final surface. The generated surface is presented below in Figure 4.4.

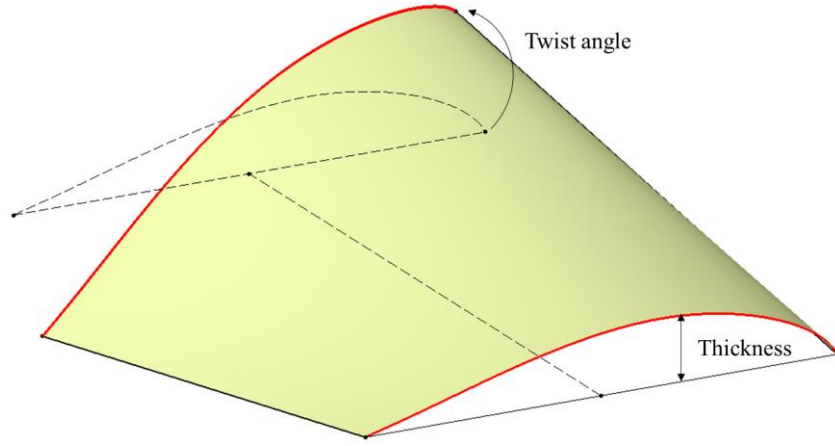


Figure 4.4: Airfoil shape with variation in thickness and twist

The final test matrix utilizing the 3 thickness and 3 twist angles is provided in Table 4.4.

Table 4.4: Test matrix for examining airfoil thickness and twist angle

ID	Thickness (%)	Twist Angle (°)
50-10	50	10
50-20	50	20
50-30	50	30
100-10	100	10
100-20	100	20
100-30	100	30
150-10	150	10
150-20	150	20
150-30	150	30

4.4 MANUFACTURABILITY RANKING STRATEGY

As mentioned in Section 3.4.2, the manufacturability scoring is highly dependent on user inputs for defect threshold and AHP matrix values. The overlap and gap thresholds are set at 25.4 mm², the angle deviation threshold is set at 2 deg, and the steering threshold

is 2000 mm. The values chosen are typical values that are of concern for each defect. Below the given values, it is assumed that the defects will have a small effect on the structural performance. The threshold values are summarized below in Table 4.5.

Table 4.5: Defect threshold values used for experiments

Defect	Threshold Value
Gap	25.4 mm ²
Overlap	25.4 mm ²
Angle Deviation	2 deg
Steering	2000 mm

All values in the AHP matrix are chosen to be 1. This will factor in each defect's instance and severity equally, leading to a scoring that incorporates all defects. All defects are to be factored equally to create a broad overview of possible issues with each investigated design. The overall rankings generated from the AHP matrix are provided in Table 4.6.

Table 4.6: AHP rankings for each defect category used for experiments

Item	Ranking
Gap Instances	0.12
Gap Severity	0.12
Overlap Instance	0.12
Overlap Severity	0.12
Angle Deviation Instances	0.12
Angle Deviation Severity	0.12
Steering Instances	0.12
Steering Severity	0.12

4.5 DIGITAL TWIN IMPLEMENTATION

Due to restrictions (COVID), limited digital twin implementation was able to be performed. However, an initial evaluation of the digital twin along with approximate simulations within the ISAAC AFP cell are possible. This also allows for testing the manufacturing data transfer and connection between neXtC and PS. Layup surfaces for the parametric studies are created and imported into the digital ISAAC AFP cell. Courses are then exported from the neXtC environment and loaded into PS for simulation. The simulation analysis consists of monitoring axis values, collision avoidance, and reachability.

4.6 SUMMARY

A parametric study is utilized to evaluate the developed data integration tools and relate manufacturability to the design parameters and tool surface. The airfoil study employs the automated tools, and further develops the capabilities of neXtC. The presented design parameters and surface features are related back to predicted defects to influence design changes. One of the airfoil surfaces is utilized to create a CAD model for the necessary tooling. This tooling is then used to generate and simulate courses. Finally, surface features are used to create an initial manufacturability approximation of the tool surface.

CHAPTER 5

EXPERIMENTATION RESULTS

5.1 STRUT EXPERIMENT RESULTS

5.1.1 MANUFACTURABILITY RESULTS

The overall manufacturability results for the 4 tow trials are shown below in Figure 5.1. Each bar represents a ply's score, while the data points show the combined laminate score. Note that the 90-degree plies are not included due to no defects being present for both the 4 tow and 2 tow trials. Initial observation of the figure shows little variation between each of the trials with slight increases in laminate scores as the transition length increases.

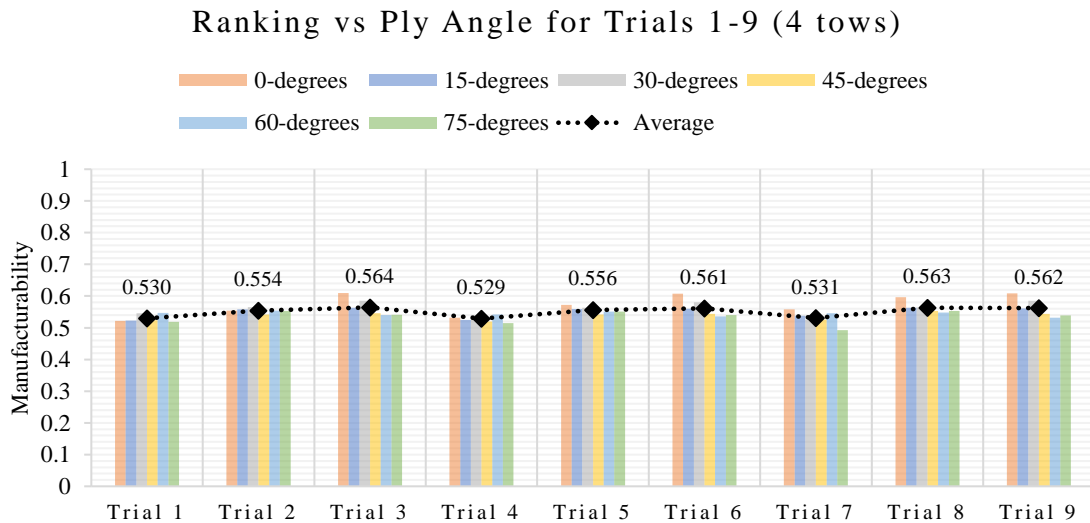


Figure 5.1: Ply and laminate scores for the 4 tow strut trials

The scores of each of the ply angles presented above are summarized in Table 5. These values are averages of the 9 trials for each angle. For the 4-tow case, the 0-degree plies performed best while the 75-degree plies performed the worse. The low scores of the 75-degree ply are attributed to an increase in defects seen in the transition zone.

Table 5.1: Average ply scores for the 4 tow strut trials

Ply Angle	Rank
0	0.573
15	0.550
30	0.561
45	0.538
60	0.544
75	0.534
*4 tows	

Similarly, the laminate average scores are presented in Table 5.2. For each radius value used, the shortest transition lengths performed the worst, while the longest transition lengths performed the best. However, the variation in scores is small and is nearly negligible.

Table 5.2: Average laminate scores for the 4 tow strut trials

Trial	Avg. Rank
Trial 1-4	0.530
Trial 2-4	0.554
Trial 3-4	0.564
Trial 4-4	0.529
Trial 5-4	0.556
Trial 6-4	0.561
Trial 7-4	0.531
Trial 8-4	0.563
Trial 9-4	0.562

Figure 5.2 below is presented to further examine the trends in how the design variables affect the manufacturability. It is seen that increasing the transition length has the largest effect on the manufacturability score. The radius values utilized have little affect regardless of which one is used, and the data is not consistent enough to draw a conclusion.

4 Tow Trial Comparisons

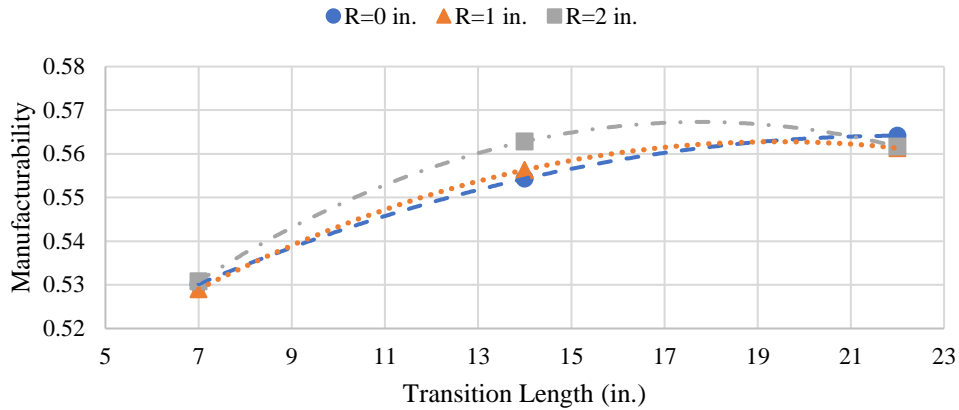


Figure 5.2: Trends in the laminate scores for the 4 tow strut trials

Similar results are acquired for the 2 tow trials. Figure 5.3 presents a summary of the results with the ply and laminate scores shown graphically. Immediately it can be seen that all the laminate scores for the 2 tow trials are lower than those seen in the 4 tow trials. The plot also shows a larger differential when increasing the transition length.

Ranking vs Ply Angle for Trials 1-9 (2 tows)

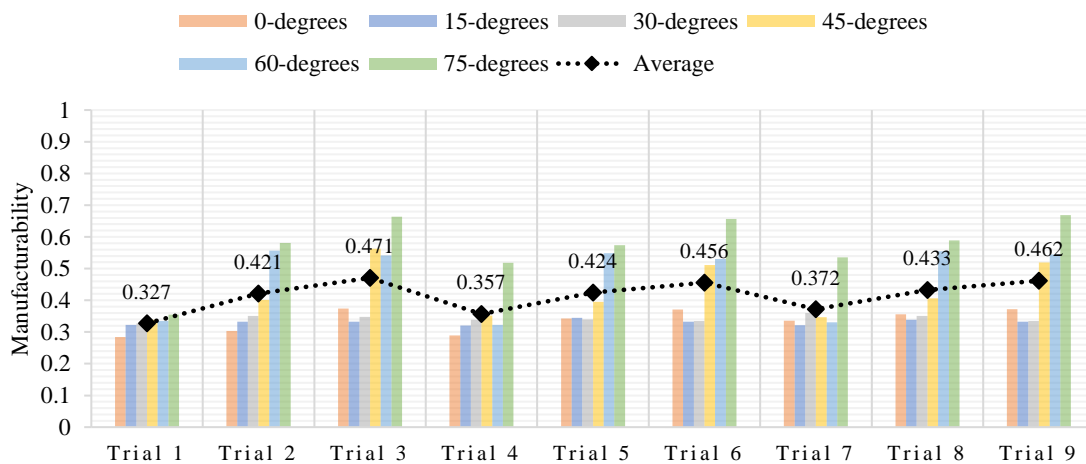


Figure 5.3: Ply and laminate score for the 2 tow strut trials

The average scores for each ply are presented below in Table 5.3. Unlike the 4 tow trials, the 75-degree ply has the best score while the 15-degree ply has the worst score. However, the plies have an overall lower score than the 4 tow trials.

Table 5.3: Average ply scores the 2 tow strut trials

Ply Angle	Rank
0	0.336
15	0.331
30	0.343
45	0.426
60	0.474
75	0.571
*2 tows	

The overall laminate score for each of the 2 tow trials is shown below in Table 5.4. These values show that a lower transition length produces a lower score while the larger lengths produce a higher score. It can also be seen that there is a larger variation in the laminates with radii values of 0 and 1 than with values of 1 and 2.

Table 5.4: Average laminate scores for the 2 tow strut trials

Trial	Avg. Rank
Trial 1-2	0.327
Trial 2-2	0.421
Trial 3-2	0.471
Trial 4-2	0.357
Trial 5-2	0.424
Trial 6-2	0.456
Trial 7-2	0.372
Trial 8-2	0.433
Trial 9-2	0.462

As before, the trends of the 2 tow trials are presented in Figure 22. The results show similar trends when compared with the 4 tow trials. In both cases, increasing the transition length leads to improved overall manufacturability scores. Also, the results from varying radius values are inconclusive with initial increases in manufacturability and the opposite effect with larger transition zones.

2 Tow Trial Comparisons

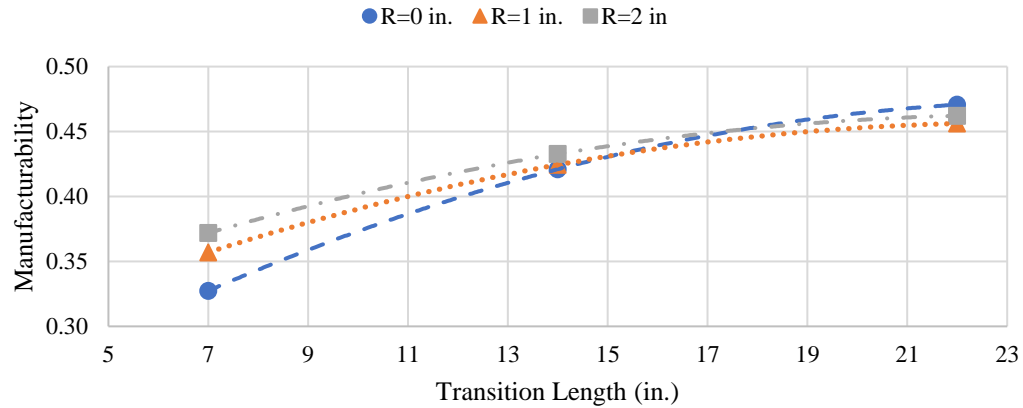


Figure 5.4: Trends in laminate scores for the 2 tow strut trials

5.1.2 DISCUSSION

The laminate scores from the trials presented above are combined and shown in Table 5.5 below. Again, all the scores from the 4 tow trials are improved when compared with those seen in the 2 tow trials. This increased score is largely due to the defects seen around the transition zone of the strut. Also, VCP checks for defects between courses therefore since more 2 tow courses are required than 4 tow courses, more zones for defects exist. Additionally, increasing the transition zone also improves the overall laminate score.

Table 5.5: Combined results for strut trials with 2 and 4 tows

	Trial 1	Trial 2	Trial 3	Trial 4	Trial 5	Trial 6	Trial 7	Trial 8	Trial 9
4 tows	0.530	0.554	0.564	0.529	0.556	0.561	0.531	0.563	0.562
2 tows	0.327	0.421	0.471	0.357	0.424	0.456	0.372	0.433	0.462

Figure 5.5 below demonstrates the difference in the defects seen in the 4 tow and 2 tow trials with an example analysis of a 45-degree ply. When manufacturing with 4 tows, the individual defect severity may be higher however the instances are significantly higher

when manufacturing with 2 tows. In the presented scoring method, this resulted in better score for the 4-tow case. While this scoring is valid for the given inputs, a further structural analysis examining these defects could be necessary. This analysis would provide a definite answer as to whether the lower defect occurrence with higher severity is a better option than increased defect occurrence with lower severity.

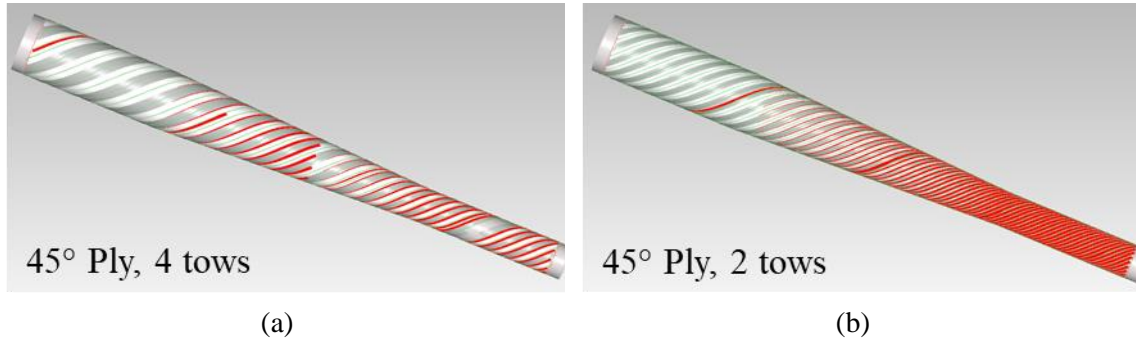


Figure 5.5: Defect analysis from VCP for 45-degree plies of (a) 4 tow and (b) 2 tow strut trials

Utilizing the presented results with additional AFP manufacturing knowledge, an optimal strut geometry design can be chosen from the analyzed profiles. From analysis of the scores, the longest transition zone (20 in.) will be the best option. Examining the scores with the individual radii does not show a clear best option. However, it is expected that a smoother transition will result in less defects due to improved roller compression and enhanced transition smoothness. These analyses result in the best geometry being a transition length of 20 in., radii of 2 in., while manufacturing with 4 tows. The selected geometry is shown in Figure 5.6 below.

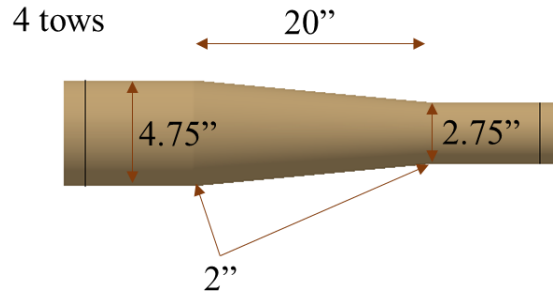


Figure 5.6: Selected strut geometry with the overall best results

5.2 AIRFOIL EXPERIMENT RESULTS

5.2.1 MANUFACTURABILITY SCORING RESULTS

Utilizing the neXtC functionalities, the manufacturability of the airfoil parametric study is analyzed. The various manufacturability characteristics of each test matrix are presented below. Along with presenting a manufacturability analysis of the given designs, the results also serve as a proof of concept of the developments of neXtC.

5.2.1.1 THICKNESS-CHORD STUDY

The preliminary results of this study showed that changing the chord length had little effect on the occurrence of defects. Throughout each trial in the test matrix, limited defects were seen across the surface with almost no effect on the manufacturability score. One results that was found was that increasing the thickness caused more steering and angle deviation defects, however they were minor. To increase the complexity of the surface, twist angles and tapers are added.

5.2.1.2 TWIST-TAPER STUDY

The overall manufacturability results of the airfoil are shown below in Figure 5.7. Each bar represents a ply's score, while the data points show the complete laminate score. Initial observation of these scores suggests that increasing twist angle lowers the manufacturability score.

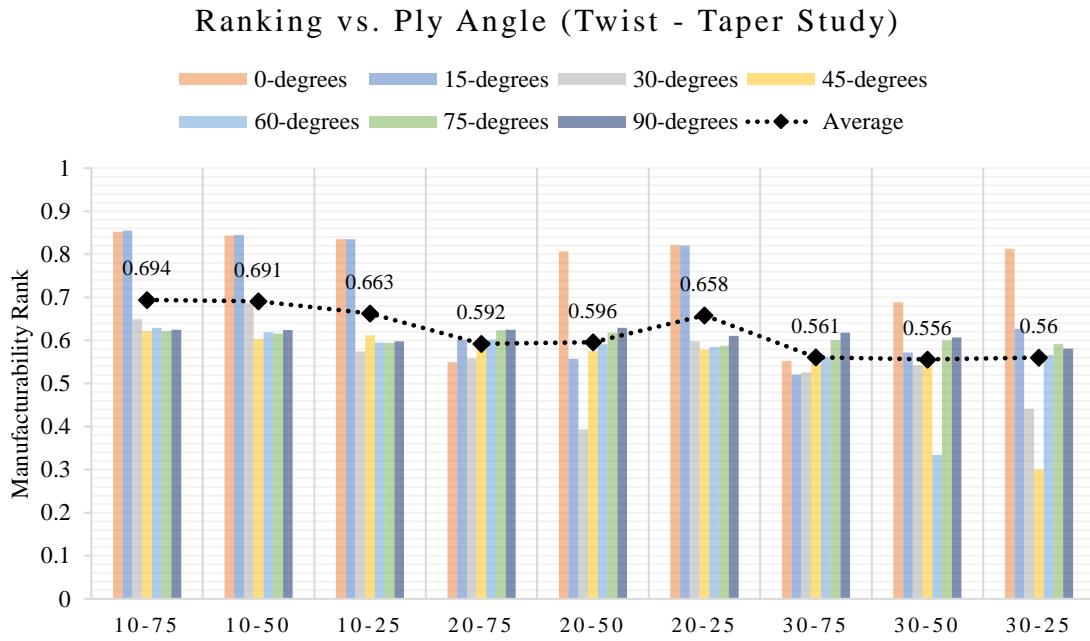


Figure 5.7: Ranking of each ply angle for the twist-taper airfoil study

The average ranking of the plies presented above are shown below in Table 5.6. This table shows that the 0-degree ply had the overall best score, while the 30- and 45-degree plies had the lowest scores.

Table 5.6: Average ply scores for airfoil twist-taper study

Twist-Taper Study	
Ply Angle	Avg. Rank
0	0.752
15	0.693
30	0.552
45	0.552
60	0.565
75	0.606
90	0.613

Similarly, the average laminate scores are presented in Table 5.7. The laminate with the lowest twist and highest taper performed the best. Each of the laminates with the highest twist performed the worst.

Table 5.7: Average laminate scores for airfoil twist-taper study

Laminate	Description (twist - taper)	Avg. Rank
L-0	10-75	0.694
L-1	10-50	0.691
L-2	10-25	0.663
L-3	20-75	0.592
L-4	20-50	0.596
L-5	20-25	0.658
L-6	30-75	0.561
L-7	30-50	0.556
L-8	30-25	0.560

Utilizing the twist, taper, and laminate manufacturability values, the graph presented in Figure 5.8 is achieved. This graph shows the correlations between the amount of twist and taper on the manufacturability score. It is seen that at the 10-degree twist, lowering the taper value results in a decreasing manufacturability score. Contrarily, the 20-degree twist results in a higher score as the taper value decreases. This is attributed to the

surface area prone to defects decreasing with the taper. Lastly, the 30-degree twist had little correlation with the taper. This extreme twist angle results in many defects that are not affected by changing the taper value.

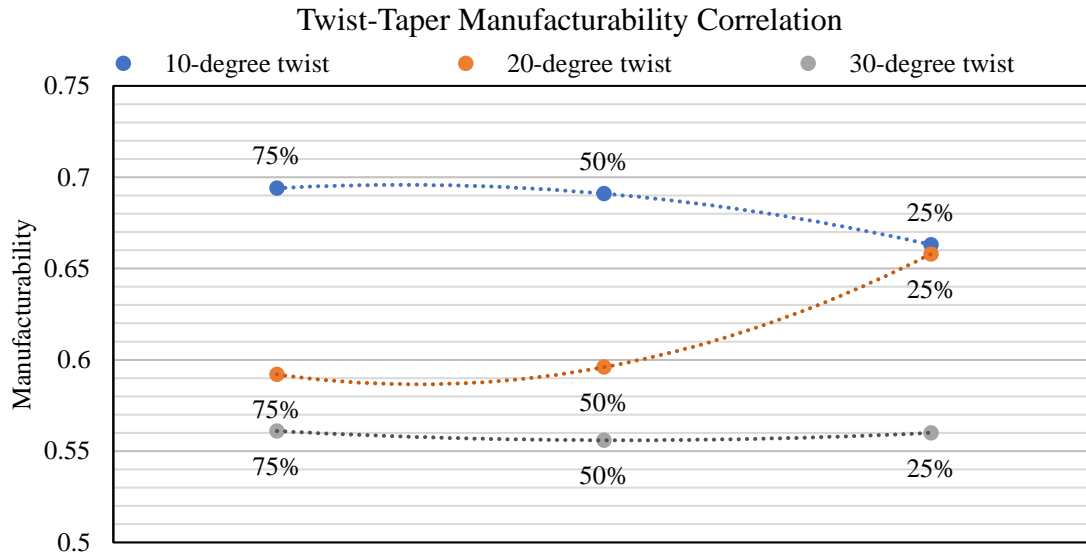


Figure 5.8: Manufacturability correlation graph for airfoil twist-taper study

5.2.1.3 THICKNESS-TWIST STUDY

Similar results are gathered for the thickness-twist parametric study. Figure 5.9 presents a summary of the results by graphically showing the ply and laminate scores. Immediately it can be seen that as the twist increases with each thickness value, the score decreases. This result compliments the ones seen above.

Ranking vs. Ply Angle (Thickness - Twist Study)

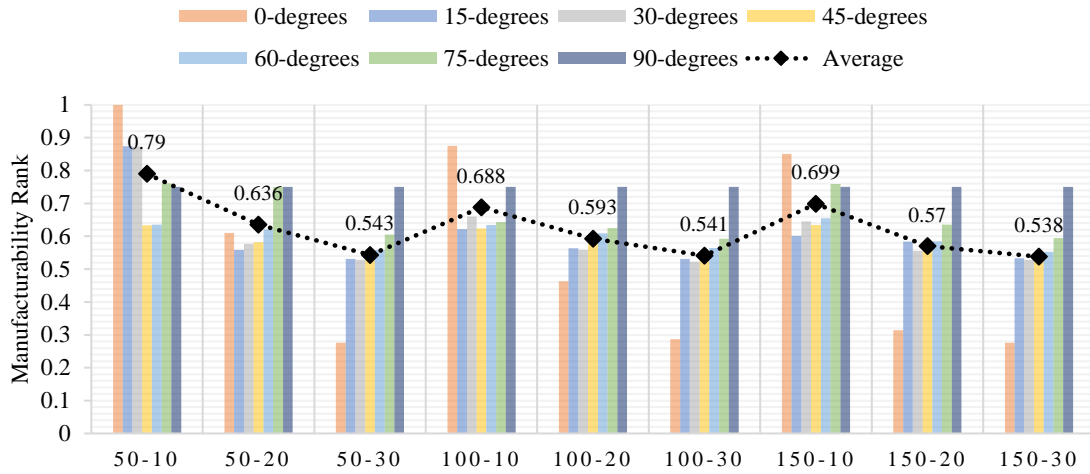


Figure 5.9: Ranking of each ply angle for the thickness-twist airfoil study

The combined average ply scores for each laminate are provided in Table 5.8. These values show that the 90-degree plies score the best, while the 0-degree plies score the worst on average.

Table 5.8: Average ply scores for airfoil thickness-twist study

Thickness-Twist Study	
Ply Angle	Rank
0	0.550
15	0.600
30	0.605
45	0.583
60	0.602
75	0.663
90	0.750

Each of the overall laminate scores is shown below in Table 5.9. The values here are the same as the average scores seen in Figure 5.9. Again, the results show that increasing the

twist angle lowers the manufacturability score. These values also show that increasing the airfoil thickness results in lower laminate scores.

Table 5.9: Average laminate scores for airfoil thickness-twist study

Laminate	Description (thickness - twist)	Avg. Rank
L-0	50-10	0.790
L-1	50-20	0.636
L-2	50-30	0.543
L-3	100-10	0.688
L-4	100-20	0.593
L-5	100-30	0.541
L-6	150-10	0.699
L-7	150-20	0.570
L-8	150-30	0.538

The correlations of the presented scores are shown below in Figure 5.10. In this case, the thickness had little effect on the trend of the scores. However, the lowest thickness value resulted in the highest initial score due to the tool surface being nearly flat. For each thickness, as the twist increases the score decreases. Each thickness value also converges near a single score for the 30-degree twist.

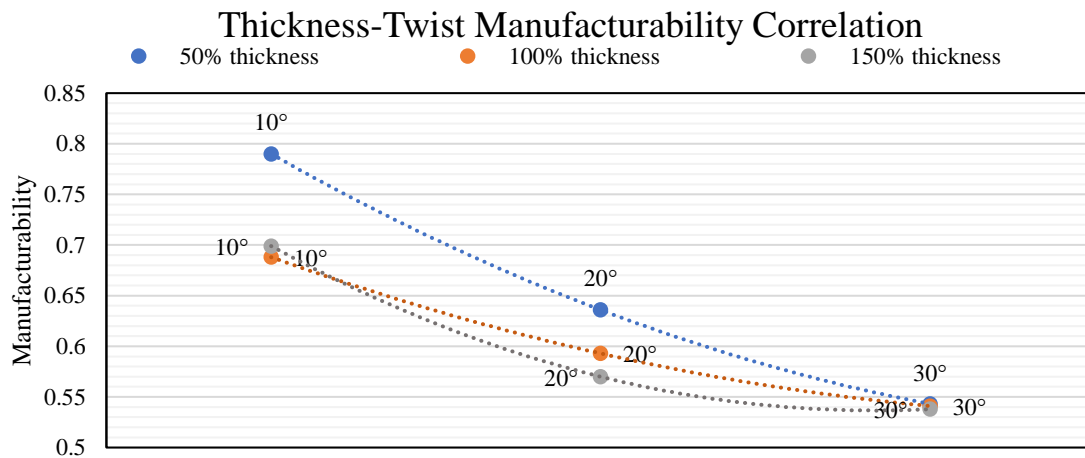


Figure 5.10: Manufacturability correlation graph for airfoil thickness-twist study

5.2.2 LOCALIZED ANALYSIS

As described in Section 3.5, neXtC performs a localized analysis to determine problems areas of the tool surface. Here, the 45-degree plies of laminate ID 100-20 (100% thickness and 20-degree twist) will be analyzed. This was chosen because the defects are representative of those seen throughout the respective trials. The results shown are extracted directly from the neXtC UI.

Figure 5.11 presents the localized analysis of the overlap, gaps, angle deviations, and steering defects. In the case of the overlap and gap defects, the values seen are percentages of the defect area with respect to the area of the local surface. The values seen in the angle deviation and steering plots are average values of the data points contained within each local surface. It should be noted that the lower values of the steering defects are worse due to the radius being closer to the critical steering radius. Analysis of the presented plots shows that most of the defects are localized near the trailing edge of the airfoil. This result is attributed to the larger changes in curvature across this section of the tool surface. However, the steering defects are worse near the middle of the tool surface. This is due to the changing curvature across the part requiring the tool paths to be steered to maintain the appropriate fiber angle. Lastly, the fiber angle deviations are not severe since the layup strategy used tries to maintain a constant angle.

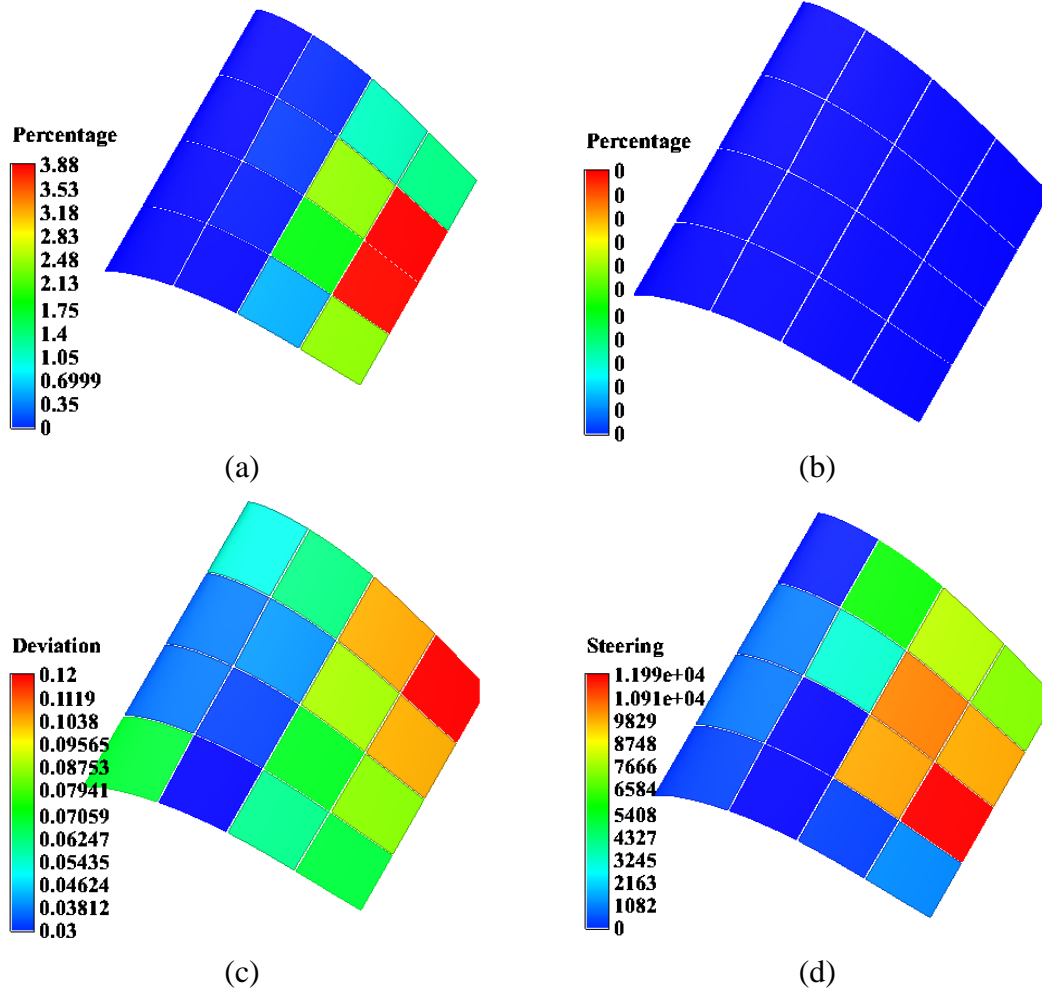


Figure 5.11: Local analysis of (a) overlaps, (b) gaps, (c) angle deviations, and (d) steering

5.2.3 ANALYSIS AND DISCUSSION

The process of finding correlations is eased by the functionalities of neXtC. Figure 5.12 presents the correlation matrix that includes the ply and laminate scores, average gaussian curvature, and the design parameters. Examination of the gaussian curvature shows that it has a strong inverse correlation with the ply and laminate scores. It also has a strong positive correlation with the twist angle. This correlation reinforces the results seen above and provides reasoning behind why the twist caused the decreasing scores.

Examining the thickness parameters shows that it has a strong inverse correlation with the 90-degree plies. This correlation is a result of steering appearing more frequently in that ply as the thickness values increased. The matrix also provides insight into which ply angles have the greatest effect on the overall laminate score. In this case, the matrix shows that the 45-degree ply has the largest effect on the overall score.

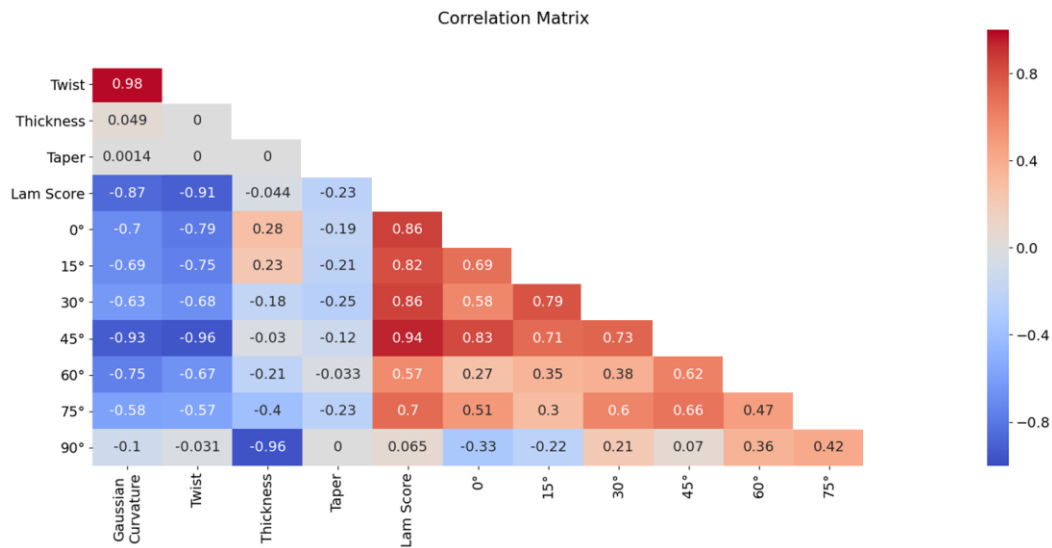


Figure 5.12: Airfoil parametric study correlation matrix

5.3 SUMMARY

The strut and airfoil parametric studies provide a manufacturability analysis that correlates surface features with defects and scores. The strut analysis demonstrated that longer transition lengths trend towards better manufacturability. These also showed that, for the specific geometry, 4 tow courses resulted in less but more severe defects when compared with the 2 tow courses. The airfoil analysis resulted in the twist angle being the largest factor in each of the scoring trials. The results also proved the design, process planning, and manufacturability functionalities of the neXtC software.

A graphical depiction of the data connection presented above is shown below in Figure 5.13. The data structure backbone of neXtC allows for design and process planning data to exist in the same environment. The data can then be analyzed together to provide a manufacturability assessment. This connection allows for the designer to understand problem areas of the designed laminate before finalizing a design for manufacturing. Such a system can eliminate the iterative process that often occurs to create a manufacturable design.

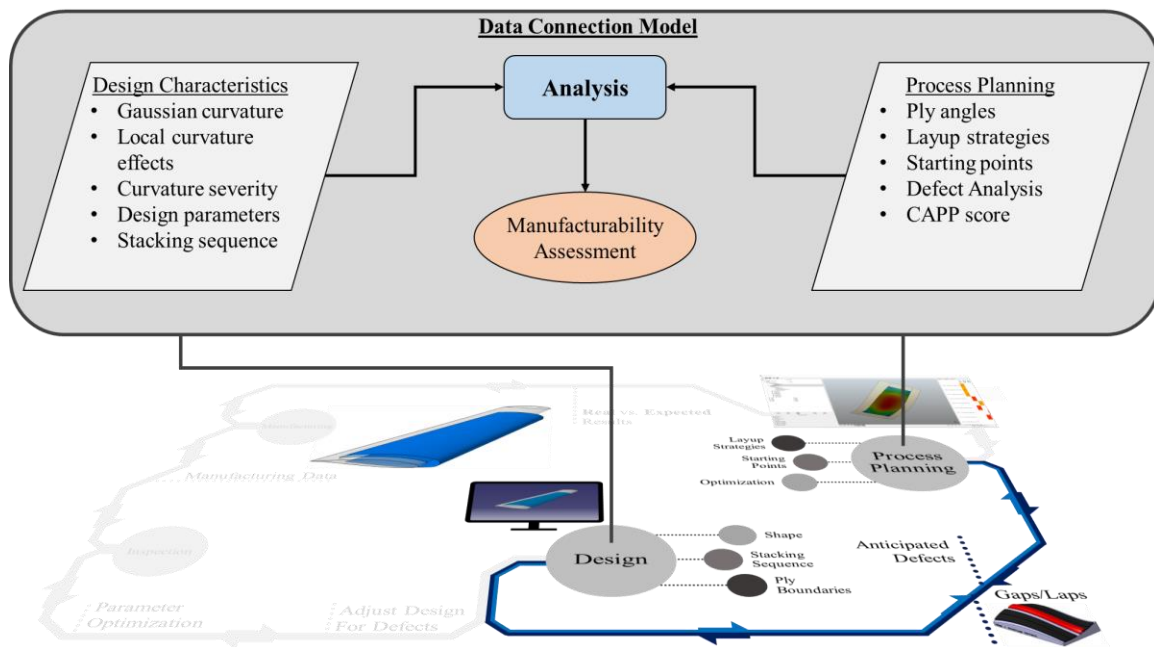


Figure 5.13: Depiction of the data connection between design and process planning

CHAPTER 6

CONCLUSIONS AND FUTURE WORK

6.1 SUMMARY OF WORK

The initiation of a software (Figure 6.1) to connect the various phases of the AFP process has been presented. The first step in this creation starts with the connection of design and process planning data to generate a manufacturability assessment. The presented functionalities achieve this by utilizing tool surface features and predicted defect data. Validation of the data connection was performed via a parametric study of a NACA 63-415 airfoil. Through the assessment, it was found that Gaussian curvature, and therefore the twist design parameter, had the largest effect on the overall manufacturability of the surface.

General manufacturability scores are found by averaging the various data points across the surface and comparing them with allowable tolerances. This analysis provides the designer with knowledge of how well the surface will perform during the manufacturing process. Localized analyses can then be used to isolate areas of the tool surface that are most problematic. The results gained can then assist in modifying the tool surface or can inform the process planner where careful action should be taken during manufacturing.

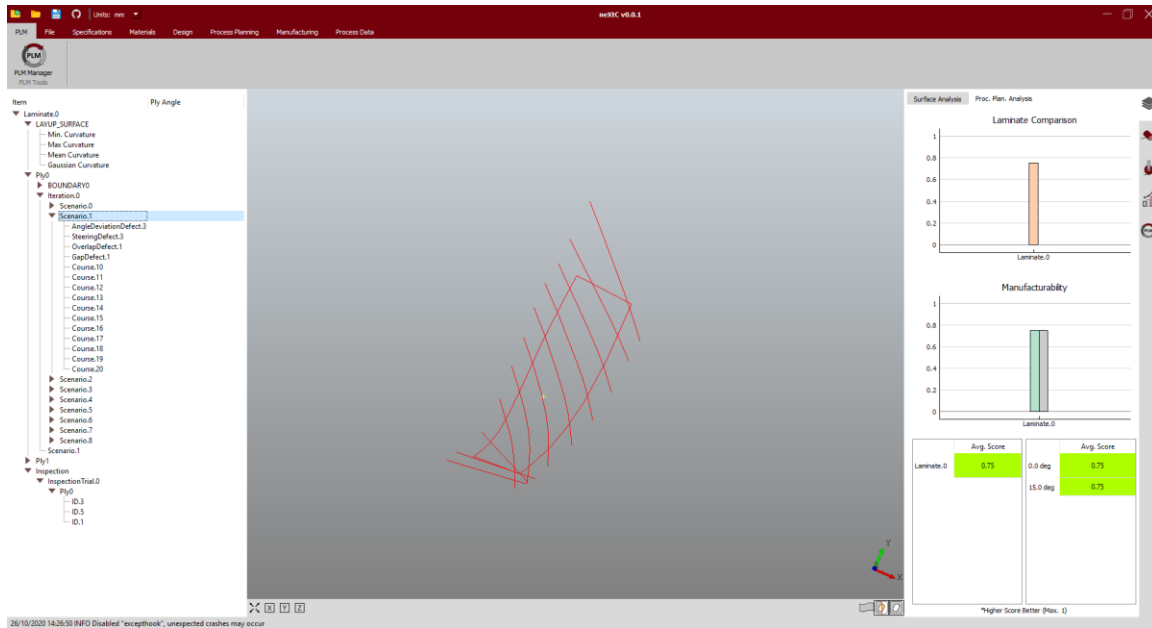


Figure 6.1: neXtC software interface

The presented data connection between the design and process planning phases of AFP is the first step in creating a closed loop PLM environment. The work in this thesis acts as an initiation of the structure needed for such an environment. As more data from the AFP lifecycle is incorporated, the PLM analysis will continually improve towards a completely closed loop system that utilizes process data to improve the AFP process.

6.2 FUTURE WORK

Development of this software has shed light on areas where further work is desired. Even at its infantile state, the desired future developments have become clear. The following will detail future work possibilities with incorporation of AFP process data. The described work will be centered on the possible outcomes of utilizing data from multiple aspects of the AFP process.

Limited design data from the entire suite of composite design was utilized in the presented work. Incorporation of strength modeling of the entire surface can provide a further assessment on how the tool surface can be adjusted to improve manufacturability. The use of such a tool should also provide suggestions on how the design can be improved. These suggestions will come from the incorporation of a large amount of the data from the design process into a model that can accurately evaluate all aspects of the design. Such a model would be able to analyze each aspect of the design and correlate it with anticipated defect occurrence from the process planning phase.

A next logical step is to analyze the relationship between the process planning data and actual manufacturing data. This creates a connection between the anticipated results and actual results, which can then be used to improve predictive models. Connection of this data can also improve the process planning phase which can now incorporate previous data to suggest possible changes that will improve the manufacturing process.

Connecting manufacturing data with inspection data provides the opportunity to connect manufacturing events with defect occurrence. The manufacturing data would consist of machine motion and parameters data that can be combined to predict defect formation based on previously seen defects. The inspection data can also be compared with anticipated defect data to analyze the predictive model. This can further improve the expected defect occurrence leading to a more realistic prediction.

6.3 SITUATION OF RESEARCH

The incorporation of the data from various aspects of the AFP lifecycle represents an overall goal of AFP research undertaken at the University of South Carolina's McNair Center. This research compliments and builds on the development of the CAPP software

by Halbritter et al. [104]. Further connection of the AFP process will be incorporated as the software develops.

REFERENCES

- [1] G. Dorey, “Carbon Fibres and Their Applications,” *J. Phys. D. Appl. Phys.*, vol. 20, no. 3, pp. 245–256, 1987.
- [2] W. Watt, L. Phillips, and W. Johnson, “High Strength High Modulus Carbon Fibres,” *Eng.*, vol. 221, p. 815, 1966, doi: 10.1016/0010-4361(92)90323-m.
- [3] W. Goldsworth and E. Hardesty, “Geodesic path length compensator for composite-tape placement head,” US3810805A, Apr. 14, 1974.
- [4] R. L. Anderson, C. G. Grant, and NASA, *Advanced fiber placement of composite fuselage structures*. in First NASA Advanced Composites Technology Conference, 1991.
- [5] D. Bullock, “Automated Prepreg Tow Placement for Composite Structures,” 1990.
- [6] C. Grant and V. Benson, “Automated Fiber Placement - Evolution and Current Demonstrations.” Accessed: Mar. 06, 2020. [Online]. Available: <https://ntrs.nasa.gov/search.jsp?R=19950022411>.
- [7] M. Enders and P. Hopkins, “Developments in the Fiber Placement Process,” 1991.
- [8] D. Evans, “Design Considerations for Fiber Placement,” 1993.
- [9] R. Measom and K. Sewell, “Fiber Placement Low-Cost Production for Complex Composite Structures.”
- [10] M. Pasanen, J. Martin, R. Langone, and J. Mondo, “Advanced Composite Fiber Placement: Process to Application,” 1997.
- [11] R. J. Cano, H. L. Belvin, A. B. Hulcher, R. W. Genoble, and R. W. Grenoble, *Studies on Automated Manufacturing of High Performance Composites*. Williamsburg, VA: in Structure Specialist Meeting, 2001.
- [12] M. B. Gruber, M. A. Lamontia, and B. J. Waibel, “AUTOMATED FABRICATION PROCESSES FOR LARGE COMPOSITE AEROSPACE STRUCTURES: A TRADE STUDY.”
- [13] A. Halbritter and R. Harper, *Big Parts Demand Big Changes to the Fiber Placement Status Quo*. Mesa, AZ: in SME Composites Manufacturing, 2012.
- [14] T. Rudberg *et al.*, *Improving AFP cell performance*, vol. 7, no. 2. in SAE International Journal of Aerospace Manufacturing and Automated Fastening, 2014.
- [15] R. Engelbart, M. Chapman, B. Johnson, K. Soucy, R. Hannebaum, and S. Schrader, “Systems and Methods Enabling Automated Return to and/or Repair of Defects with a Material Placement Machine,” US7039485B2, 2004.

- [16] R. Devlieg, K. Jeffries, and P. Vogeli, "High-speed fiber placement on large complex structures," 2007, doi: 10.4271/2007-01-3843.
- [17] R. Flynn, J. Nielson, and T. Rudberg, "Production Implementation of Multiple Machine, High Speed Fiber Placement for Large Structures," Electroimpact, Inc, 2010.
- [18] K. A. Jeffries, "Enhanced Robotic Automated Fiber Placement with Accurate Robot Technology and Modular Fiber Placement Head," *SAE Int. J. Aerosp.*, vol. 6, no. 2, pp. 774–779, 2013, doi: 10.4271/2013-01-2290.
- [19] R. Harik, *Automated Fiber Placement: Status, Challenges and Evolutions (Submitted)*. SAE, 2021.
- [20] R. Harik, "neXt Automated Fiber Placement: Advancing Composites Manufacturing Towards a New Paradigm," *SAMPE Journal*, pp. 6–14, 2020.
- [21] S. W. Beckwith, "Designing with Composites: Suggested 'Best Practices' Rules," *SAMPE J.*, vol. 45, no. 1, p. 17, 2009.
- [22] S. Setoodeh, M. M. Abdalla, and Z. Gürdal, "Design of variable-stiffness laminates using lamination parameters," *Compos. Part B Eng.*, vol. 37, no. 4–5, pp. 301–309, Jun. 2006, doi: 10.1016/j.compositesb.2005.12.001.
- [23] H. Ghiasi, D. Pasini, and L. Lessard, "Optimum stacking sequence design of composite materials Part I: Constant stiffness design," *Composite Structures*, vol. 90, no. 1, pp. 1–11, Sep. 2009, doi: 10.1016/j.compstruct.2009.01.006.
- [24] H. Ghiasi, K. Fayazbakhsh, D. Pasini, and L. Lessard, "Optimum stacking sequence design of composite materials Part II: Variable stiffness design," *Composite Structures*, vol. 93, no. 1, Elsevier, pp. 1–13, Dec. 01, 2010, doi: 10.1016/j.compstruct.2010.06.001.
- [25] M. A. Albazzan, R. Harik, B. F. Tatting, and Z. Gürdal, "Efficient design optimization of nonconventional laminated composites using lamination parameters: A state of the art," *Composite Structures*, vol. 209, Elsevier Ltd, pp. 362–374, Feb. 01, 2019, doi: 10.1016/j.compstruct.2018.10.095.
- [26] M. A. Albazzan *et al.*, "Optimization of cylinders with holes under bending using nonconventional laminates," 2018, doi: 10.2514/6.2018-1377.
- [27] M. Arian Nik, K. Fayazbakhsh, D. Pasini, and L. Lessard, "Surrogate-based multi-objective optimization of a composite laminate with curvilinear fibers," *Compos. Struct.*, vol. 94, no. 8, pp. 2306–2313, Jul. 2012, doi: 10.1016/j.compstruct.2012.03.021.
- [28] M. Arian Nik, K. Fayazbakhsh, D. Pasini, and L. Lessard, "Optimization of variable stiffness composites with embedded defects induced by Automated Fiber Placement," *Compos. Struct.*, vol. 107, no. 1, pp. 160–166, Jan. 2014, doi: 10.1016/j.compstruct.2013.07.059.
- [29] G. Huang, H. Wang, and G. Li, "An efficient reanalysis assisted optimization for variable-stiffness composite design by using path functions," *Compos. Struct.*, vol. 153, pp. 409–420, Oct. 2016, doi: 10.1016/j.compstruct.2016.06.043.

- [30] E. Lemaire, S. Zein, and M. Bruyneel, "Optimization of composite structures with curved fiber trajectories," *Compos. Struct.*, vol. 131, pp. 895–904, Nov. 2015, doi: 10.1016/j.compstruct.2015.06.040.
- [31] D. C. Jegley, B. F. Tatting, and Z. Gürdal, "Optimization of elastically tailored tow-placed plates with holes," in *Collection of Technical Papers - AIAA/ASME/ASCE/AHS/ASC Structures, Structural Dynamics and Materials Conference*, 2003, vol. 1, pp. 205–218, doi: 10.2514/6.2003-1420.
- [32] G. Rousseau, R. Wehbe, J. Halbritter, and R. Harik, "Automated fiber placement path planning: A state-of-the-art review," *Comput. Aided. Des. Appl.*, vol. 16, no. 2, pp. 172–203, 2019, doi: 10.14733/cadaps.2019.172-203.
- [33] L. Li, X. Wang, D. Xu, and M. Tan, "A Placement Path Planning Algorithm Based on Meshed Triangles for Carbon Fiber Reinforce Composite Component with Revolved Shape," *Int. J. Control Syst. Appl.*, vol. 1, no. 1, 2014.
- [34] M. Favaloro and D. Hauber, "Process and design considerations for the automated fiber placement process | Request PDF," 2007, Accessed: May 27, 2020. [Online]. Available: https://www.researchgate.net/publication/286730547_Process_and_design_considerations_for_the_automated_fiber_placement_process/citations.
- [35] K. Schueler, J. Miller, and R. Hale, "Approximate geometric methods in application to the modeling of fiber placed composite structures," *J. Comput. Inf. Sci. Eng.*, vol. 4, no. 3, pp. 251–256, Sep. 2004, doi: 10.1115/1.1736685.
- [36] B. Shirinzadeh, G. Cassidy, D. Oetomo, G. Alici, and M. H. Ang, "Trajectory generation for open-contoured structures in robotic fibre placement," *Robot. Comput. Integr. Manuf.*, vol. 23, no. 4, pp. 380–394, Aug. 2007, doi: 10.1016/j.rcim.2006.04.006.
- [37] N. Patrikalakis and T. Maekawa, *Shape Interrogation or Computer Aided Design and Manufacturing*. Springer Science & Business Media, 2002.
- [38] Z. Gürdal, B. F. Tatting, and K. Chauncey Wu, "Tow-placement technology and fabrication issues for laminated composite structures," in *Collection of Technical Papers - AIAA/ASME/ASCE/AHS/ASC Structures, Structural Dynamics and Materials Conference*, 2005, vol. 4, pp. 2716–2733, doi: 10.2514/6.2005-2017.
- [39] E. Beyeler, W. Phillips, and S. I. Güçeri, "Experimental Investigation of Laser-Assisted Thermoplastic Tape Consolidation," *J. Thermoplast. Compos. Mater.*, vol. 1, no. 1, pp. 107–121, Jan. 1988, doi: 10.1177/089270578800100109.
- [40] "Laser Processing of Thermoplastic Composites | Automated Dynamics - Composite Structures, Automation Equipment, and Engineering Services." <http://www.automateddynamics.com/article/thermoplastic-composite-basics/processing-methods/laser-processing-of-thermoplastic-composites> (accessed Jul. 21, 2020).
- [41] Z. Qureshi, T. Swait, R. Scaife, and H. M. El-Dessouky, "In situ consolidation of thermoplastic prepreg tape using automated tape placement technology: Potential and possibilities," *Compos. Part B Eng.*, vol. 66, pp. 255–267, Nov. 2014, doi:

10.1016/j.compositesb.2014.05.025.

- [42] “Intelligent heat for Automated Fibre Placement.” Heraeus Noblelight Limited.
- [43] R. Flynn, T. Rudberg, and J. Stamen, “Automated Fiber Placement Machine Developments: Modular Heads, Tool Point Programming and Volumetric Compensation Bring New Flexibility in a Scalable AFP Cell,” 2011.
- [44] J. T. Quinlivan and H. R. Fenbert, “Composite Applications in Commercial Transport Aircraft,” in *Polymers and Other Advanced Materials*, Springer US, 1995, pp. 1–5.
- [45] B. N. Bhat, F. E. Ledbetter, and G. C. Marshall, “Materials and processing technologies for highly reusable vehicles and propulsion systems,” 1997, doi: 10.2514/6.1997-2857.
- [46] J. Kelly, G. Leon, J. Hall, and C. Woodall, “Reliable Design and Fabrication of Composite High Performance Marine Structures,” 1995.
- [47] A. W. Blom, M. M. Abdalla, and Z. Gürdal, “Optimization of course locations in fiber-placed panels for general fiber angle distributions,” *Compos. Sci. Technol.*, vol. 70, no. 4, pp. 564–570, Apr. 2010, doi: 10.1016/j.compscitech.2009.12.003.
- [48] M. Bruyneel and S. Zein, “A modified Fast Marching Method for defining fiber placement trajectories over meshes,” *Comput. Struct.*, vol. 125, pp. 45–52, Sep. 2013, doi: 10.1016/j.compstruc.2013.04.015.
- [49] C. J. Brampton and H. A. Kim, “Optimization of Tow Steered Fiber Orientation Using the Level Set Method,” 2013.
- [50] B. C. Kim, K. Hazra, P. Weaver, and K. Potter, “Limitations of Fibre Placement Techniques for Variable Angle Tow Composites and Their Process-Induced Defects,” 2011.
- [51] A. W. Blom, C. S. Lopes, P. J. Kromwijk, Z. Gürdal, and P. P. Camanho, “A theoretical model to study the influence of tow-drop areas on the stiffness and strength of variable-stiffness laminates,” *J. Compos. Mater.*, vol. 43, no. 5, pp. 403–425, Mar. 2009, doi: 10.1177/0021998308097675.
- [52] M. Jiang, B. Wu, and F. Li, “Path optimization for open-contoured structures in Robotic Fibre Placement,” in *Proceedings - 2017 32nd Youth Academic Annual Conference of Chinese Association of Automation, YAC 2017*, Jun. 2017, pp. 207–212, doi: 10.1109/YAC.2017.7967406.
- [53] M. H. FarzanehKaloorazi, I. A. Bonev, and L. Birglen, “Simultaneous path placement and trajectory planning optimization for a redundant coordinated robotic workcell,” *Mech. Mach. Theory*, vol. 130, pp. 346–362, Dec. 2018, doi: 10.1016/j.mechmachtheory.2018.08.022.
- [54] S. Lei, “Simulation based optimization on automated fibre placement process,” in *IOP Conference Series: Materials Science and Engineering*, Feb. 2018, vol. 307, no. 1, doi: 10.1088/1757-899X/307/1/012001.
- [55] M. A. Khan, P. Mitschang, and R. Schledjewski, “Parametric study on processing

- parameters and resulting part quality through thermoplastic tape placement process,” *J. Compos. Mater.*, vol. 47, no. 4, pp. 485–499, Feb. 2013, doi: 10.1177/0021998312441810.
- [56] M. Nagelsmith and W. Guerrits, “Influence of steering radius on the mechanical properties of fiber placed composite laminates,” 2013.
 - [57] E. Oromiehie, B. G. Prusty, P. Compston, and G. Rajan, “The influence of consolidation force on the performance of AFP manufactured laminates,” in *ICCM International Conferences on Composite Materials*, 2017, vol. 2017-Augus, Accessed: Feb. 19, 2020. [Online]. Available: <https://ro.uow.edu.au/eispapers1https://ro.uow.edu.au/eispapers1/1810>.
 - [58] R. Engelhardt, R. Irmanputra, K. Brath, N. Aufenanger, and K. Drechsler, “Thermoset Prepreg Compaction during Automated Fiber Placement and Vacuum Debulking,” *Procedia CIRP*, vol. 85, pp. 153–158, Jan. 2019, doi: 10.1016/j.procir.2019.09.025.
 - [59] J. Chen, T. Chen-Keat, M. Hojjati, A. Vallee, M. A. Oceau, and A. Yousefpour, “Impact of layup rate on the quality of fiber steering/cut-restart in automated fiber placement processes,” *Sci. Eng. Compos. Mater.*, vol. 22, no. 2, pp. 165–173, Mar. 2015, doi: 10.1515/secm-2013-0257.
 - [60] M. A. Khan, P. Mitschang, and R. Schledjewski, “Identification of some optimal parameters to achieve higher laminate quality through tape placement process,” *Adv. Polym. Technol.*, vol. 29, no. 2, pp. 98–111, Jun. 2010, doi: 10.1002/adv.20177.
 - [61] M. Belhaj *et al.*, “Dry fiber automated placement of carbon fibrous preforms,” *Compos. Part B Eng.*, vol. 50, pp. 107–111, Jul. 2013, doi: 10.1016/j.compositesb.2013.01.014.
 - [62] F. K. D and S. K. V, “A New Compact Robotic Head for Thermoplastic Fiber Placement,” *Int. SAMPE Symp. Exhib. (Society Adv. Mater. Process Eng.*, vol. 38, no. 1, pp. 138–151, 1993, Accessed: Jul. 21, 2020. [Online]. Available: https://jglobal.jst.go.jp/en/detail?JGLOBAL_ID=200902189958781145.
 - [63] D. Saenz, D. S. Del Castillo, I. Martin, F. Rodriguez-Lence, and A. Guemes, “On-line monitoring of a laser-Assisted fiber placement process with CFR thermoplastic matrix by using Fiber Bragg Gratings,” 2016, Accessed: Feb. 19, 2020. [Online]. Available: <http://www.ndt.net/?id=20174>.
 - [64] T. T. Zacchia, F. Shadmehri, J. Fortin-Simpson, and S. Van Hoa, “Design of Hard Compaction Rollers for Automated Fiber Placement on Complex Mandrel Geometries,” in *Proceedings of The Canadian Society for Mechanical Engineering International Congress 2018*, 2018, pp. 1–4, doi: 10.25071/10315/35245.
 - [65] C. Schmidt, B. Denkena, T. Hocke, and K. Völtzer, “Influence of AFP Process Parameters on the Temperature Distribution Used for Thermal in-process Monitoring,” in *1st Cirp Conference on Composite Materials Parts Manufacturing*, 2017, vol. 66, pp. 68–73, doi: 10.1016/j.procir.2017.03.220.
 - [66] P. M. Schaefer, D. Gierszewski, A. Kollmannsberger, S. Zaremba, and K. Drechsler, “Analysis and improved process response prediction of laser- assisted automated

tape placement with PA-6/carbon tapes using Design of Experiments and numerical simulations,” *Compos. Part A Appl. Sci. Manuf.*, vol. 96, pp. 137–146, May 2017, doi: 10.1016/j.compositesa.2017.02.008.

- [67] P. E. Bourban, N. Bernet, J. E. Zanetto, and J. A. E. Månson, “Material phenomena controlling rapid processing of thermoplastic composites,” *Compos. - Part A Appl. Sci. Manuf.*, vol. 32, no. 8, pp. 1045–1057, Aug. 2001, doi: 10.1016/S1359-835X(01)00017-3.
- [68] T. G. Gutowski, *Advanced Composites Manufacturing*. John Wiley & Sons, 1997.
- [69] F. O. Sonmez and H. T. Hahn, “Analysis of the On-Line Consolidation Process in Thermoplastic Composite Tape Placement,” *J. Thermoplast. Compos. Mater.*, vol. 10, no. 6, pp. 543–572, Nov. 1997, doi: 10.1177/089270579701000604.
- [70] F. O. Sonmez and H. T. Hahn, “Modeling of Heat Transfer and Crystallization in Thermoplastic Composite Tape Placement Process,” *J. Thermoplast. Compos. Mater.*, vol. 10, no. 3, pp. 198–240, May 1997, doi: 10.1177/089270579701000301.
- [71] F. O. Sonmez, H. T. Hahn, and M. Akbulut, “Analysis of Process-Induced Residual Stresses in Tape Placement,” *J. Thermoplast. Compos. Mater.*, vol. 15, no. 6, pp. 525–544, Nov. 2002, doi: 10.1177/0892705702015006207.
- [72] J. J. Tierney and J. W. Gillespie, “Crystallization kinetics behavior of PEEK based composites exposed to high heating and cooling rates,” *Compos. Part A Appl. Sci. Manuf.*, vol. 35, no. 5, pp. 547–558, May 2004, doi: 10.1016/j.compositesa.2003.12.004.
- [73] M. A. Khan, P. Mitschang, and R. Schledjewski, “Tracing the Void Content Development and Identification of its Effecting Parameters during in Situ Consolidation of Thermoplastic Tape Material,” *Polym. Polym. Compos.*, vol. 18, no. 1, pp. 1–15, Jan. 2010, doi: 10.1177/096739111001800101.
- [74] S. Ranganathan, S. G. Advani, and M. A. Lamontia, “A Non-Isothermal Process Model for Consolidation and Void Reduction during In-Situ Tow Placement of Thermoplastic Composites,” *J. Compos. Mater.*, vol. 29, no. 8, pp. 1040–1062, May 1995, doi: 10.1177/002199839502900803.
- [75] F. Yang and R. Pitchumani, “Nonisothermal healing and interlaminar bond strength evolution during thermoplastic matrix composites processing,” *Polym. Compos.*, vol. 24, no. 2, pp. 263–278, Apr. 2003, doi: 10.1002/pc.10027.
- [76] S. C. Mantell and G. S. Springer, “Manufacturing Process Models for Thermoplastic Composites,” *J. Compos. Mater.*, vol. 26, no. 16, pp. 2348–2377, Jan. 1992, doi: 10.1177/002199839202601602.
- [77] K. J. Ahn, J. C. Seferis, T. Pelton, and M. Wilhelm, “Analysis and characterization of prepreg tack,” *Polym. Compos.*, vol. 13, no. 3, pp. 197–206, 1992, doi: 10.1002/pc.750130308.
- [78] O. Dubois, J. B. Le Cam, and A. Béakou, “Experimental analysis of prepreg tack,” *Exp. Mech.*, vol. 50, no. 5, pp. 599–606, Jun. 2010, doi: 10.1007/s11340-009-9236-7.

- [79] R. J. Crossley, P. J. Schubel, and N. A. Warrior, "The experimental determination of prepreg tack and dynamic stiffness," *Compos. Part A Appl. Sci. Manuf.*, vol. 43, no. 3, pp. 423–434, Mar. 2012, doi: 10.1016/j.compositesa.2011.10.014.
- [80] R. J. Crossley, P. J. Schubel, and D. S. A. De Focatiis, "Time-temperature equivalence in the tack and dynamic stiffness of polymer prepreg and its application to automated composites manufacturing," *Compos. Part A Appl. Sci. Manuf.*, vol. 52, pp. 126–133, Sep. 2013, doi: 10.1016/j.compositesa.2013.05.002.
- [81] A. Endruweit, D. S. A. De Focatiis, S. Ghose, B. A. Johnson, D. R. Younkin, and N. A. Warrior, "Characterization of prepreg tack to aid automated material placement," 2016.
- [82] A. Endruweit *et al.*, "Characterisation of tack for uni-directional prepreg tape employing a continuous application-and-peel test method," *Compos. Part A Appl. Sci. Manuf.*, vol. 114, pp. 295–306, Nov. 2018, doi: 10.1016/j.compositesa.2018.08.027.
- [83] W. Zhang, F. Liu, Y. Lv, and X. Ding, "Modelling and layout design for an automated fibre placement mechanism," *Mech. Mach. Theory*, vol. 144, Feb. 2020, doi: 10.1016/j.mechmachtheory.2019.103651.
- [84] M. Assadi and T. Field, "AFP Processing of Dry Fiber Carbon Materials (DFP) for Improved Rates and Reliability," *SAE Tech. Pap.*, 2020, doi: 10.4271/2020-01-0030.
- [85] T. Rudberg, J. Cemenska, and E. Sherrard, "A Process for Delivering Extreme AFP Head Reliability," *SAE Tech. Pap.*, 2019, doi: 10.4271/2019-01-1349.
- [86] T. Aized and B. Shirinzadeh, "Robotic fiber placement process analysis and optimization using response surface method," *Int. J. Adv. Manuf. Technol.*, vol. 55, no. 1–4, pp. 393–404, Jul. 2011, doi: 10.1007/s00170-010-3028-1.
- [87] Z. Han, S. Sun, Z. Shao, and H. Fu, "Multiscale Collaborative Optimization of Processing Parameters for Carbon Fiber/Epoxy Laminates Fabricated by High-Speed Automated Fiber Placement," *Adv. Mater. Sci. Eng.*, 2016, doi: 10.1155/2016/5480352.
- [88] R. Wehbe, C. Sacco, A. Baz Radwan, M. Albazzan, and R. Harik, "Influence of process parameters in AFP fiber steering on cylinders: Constant curvature paths," *Compos. Part C Open Access*, vol. 2, p. 100036, Oct. 2020, doi: 10.1016/j.jcomc.2020.100036.
- [89] K. Croft, L. Lessard, D. Pasini, M. Hojjati, J. Chen, and A. Yousefpour, "Experimental study of the effect of automated fiber placement induced defects on performance of composite laminates," *Compos. Part A Appl. Sci. Manuf.*, vol. 42, no. 5, pp. 484–491, May 2011, doi: 10.1016/j.compositesa.2011.01.007.
- [90] A. Rafal *et al.*, "An experimental investigation concerning the effects of AFP defects on progressive failure of tensile coupons," in *AIAA Scitech 2019 Forum*, 2019, pp. 1–9, doi: 10.2514/6.2019-1547.
- [91] R. Harik, Z. Gurdal, C. Saidy, S. J. Williams, and B. Grimsley, "Automated Fiber

Placement Defect Identity Cards: Cause, Anticipation, Existence, Significance, and Progression,” 2018, Accessed: Mar. 25, 2020. [Online]. Available: <https://www.researchgate.net/publication/326464139>.

- [92] B. Denkena, C. Schmidt, K. Völtzer, and T. Hocke, “Thermographic online monitoring system for Automated Fiber Placement processes,” *Compos. Part B Eng.*, vol. 97, pp. 239–243, Jul. 2016, doi: 10.1016/j.compositesb.2016.04.076.
- [93] A. Brasington, T. Schachner, and R. Harik, “3D Modeling and Printing of Automated Fiber Placement Defects,” 2020.
- [94] A. T. Noever, C. S. Collier, R. Harik, and J. Halbritter, “Development of a Design for Manufacturing Tool for Automated Fiber Placement Structures,” in *AIAA Scitech 2019 Forum*, 2019, p. 0520.
- [95] A. Noever, C. Collier, and R. Harik, “Integrated Design and Manufacturing Analysis for Automated Fiber Placement Structures,” 2019.
- [96] A. E. Burov and O. G. Burova, “Development of digital twin for composite pressure vessel,” in *Journal of Physics: Conference Series*, Jan. 2020, vol. 1441, doi: 10.1088/1742-6596/1441/1/012133.
- [97] G. Seon, Y. Nikishkov, A. Makeev, and L. Ferguson, “Towards a digital twin for mitigating void formation during debulking of autoclave composite parts,” *Eng. Fract. Mech.*, vol. 225, p. 106792, Feb. 2020, doi: 10.1016/j.engfracmech.2019.106792.
- [98] W. Polini and A. Corrado, “Digital twin of composite assembly manufacturing process,” *Int. J. Prod. Res.*, vol. 58, no. 17, pp. 5238–5252, Sep. 2020, doi: 10.1080/00207543.2020.1714091.
- [99] D. J. Hughes, S. Keir, and C. Meggs, “Digital Twin Methodology for Compression Moulded Thermoplastic Composite Optimisation,” 2018.
- [100] E. H. Glaessgen and D. S. Stargel, “The digital twin paradigm for future NASA and U.S. Air force vehicles,” 2012, doi: 10.2514/6.2012-1818.
- [101] F. Tao, J. Cheng, Q. Qi, M. Zhang, H. Zhang, and F. Sui, “Digital twin-driven product design, manufacturing and service with big data,” *Int. J. Adv. Manuf. Technol.*, vol. 94, no. 9–12, pp. 3563–3576, Feb. 2018, doi: 10.1007/s00170-017-0233-1.
- [102] R. Rosen, G. Von Wichert, G. Lo, and K. D. Bettenhausen, “About the importance of autonomy and digital twins for the future of manufacturing,” in *IFAC-PapersOnLine*, May 2015, vol. 28, no. 3, pp. 567–572, doi: 10.1016/j.ifacol.2015.06.141.
- [103] B. Schleich, N. Anwer, L. Mathieu, and S. Wartzack, “Shaping the digital twin for design and production engineering,” *CIRP Ann. - Manuf. Technol.*, vol. 66, pp. 141–144, Jan. 2017, doi: 10.1016/j.cirp.2017.04.040.
- [104] J. A. Halbritter, “Automation of Process Planning for Automated Fiber Placement,” University of South Carolina, 2020.

- [105] M. Kirkpatrick *et al.*, “Creation of a Digital Twin for Automated Fiber Placement,” 2020.